CERN-TH.7346/94

Towards a Model-Independent Analysis of Rare B Decays

A. Ali[1], G.F. Giudice[2], and T. Mannel

Theory Division, CERN
CH-1211 Geneva 23, Switzerland

Abstract

Motivated by the experimental accessibility of rare B decays in the ongoing and planned experiments, we propose to undertake a model-independent analysis of the inclusive decay rates and distributions in the processes $B \to X_s\gamma$ and $B \to X_s\ \ell^+\ell^-$ ($B = B^\pm$ or B_d^0). We show how measurements of the decay rates and distributions in these processes would allow us to extract the magnitude and sign of the dominant Wilson coefficients of the magnetic moment operator $m_b\bar{s}_L\sigma_{\mu\nu}b_RF^{\mu\nu}$ and the four-fermion operators $(\bar{s}_L\gamma_\mu b_L)(\bar{\ell}\gamma^\mu\ell)$ and $(\bar{s}_L\gamma_\mu b_L)(\bar{\ell}\gamma^\mu\gamma^5\ell)$. Non-standard-model effects could thus manifest themselves at low energy in rare B decays through the Wilson coefficient having values distinctly different from their standard-model counterparts. We illustrate this possibility using the examples of the two-doublet Higgs models and the minimal supersymmetric models. The dilepton invariant mass spectrum and the forward-backward asymmetry of ℓ^+ in the centre-of-mass system of the dilepton pair in the decay $B \to X_s\ \ell^+\ell^-$ are also worked out for the standard model and some representative solutions for the other two models.

CERN-TH.7346/94
July 1994

[1]On leave of absence from DESY, Hamburg, FRG.
[2]On leave of absence from INFN, Sezione di Padova, Italy.

1 Introduction

The measurement of the decay mode $B \to K^*\gamma$ by the CLEO collaboration [1], having a branching ratio $\mathcal{B}(B \to K^*\gamma) = (4.5 \pm 1.0 \pm 0.9) \times 10^{-5}$, has put the physics of the electromagnetic penguins on an experimental footing.This measurement and the experimental upper bound on the inclusive decay $\mathcal{B}(B \to X_s\gamma) < 5.4 \times 10^{-4}$ at 90% C.L. [2] have been analysed in the context of the standard model (SM) [3] and in extensions of it such as the two-Higgs-doublet models (2HDM) [4, 5, 6], the minimal supersymmetric models (MSSM) [7, 8, 9], and a number of other more exotic variations [10, 11]. Very recently, the CLEO collaboration has published a first measurement of the inclusive decay rate, based on the measurement of the photon energy spectrum in the decay $B \to X_s\gamma$ [12]. The branching ratio

$$\mathcal{B}(B \to X_s\gamma) = (2.32 \pm 0.51 \pm 0.32 \pm 0.20) \times 10^{-4} \tag{1}$$

puts more restrictive bounds on the non-SM parameters. In the SM context, the short-distance contributions in these transitions are dominated by the top quark and hence they provide valuable information about its mass and the Cabibbo-Kobayashi-Maskawa (CKM) weak mixing matrix elements $V_{ts}V_{tb}$ [13]. Specifically, the recent CLEO measurement of $\mathcal{B}(B \to X_s\gamma)$ yields at present the following bounds [3]:

$$0.62 \leq \left|\frac{V_{ts}}{V_{cb}}\right| \leq 1.1 \ . \tag{2}$$

Alternatively, the ratio V_{ts}/V_{cb} can be determined from unitarity and one may use $|V_{ts}|/|V_{cb}| \simeq 1$ to obtain from the CLEO measurements bounds on the Wilson coefficient $C_7(m_b)$ of the effective magnetic moment operator. Using $\mathcal{B}(B \to X_s\gamma) = (2.32 \pm 0.67) \times 10^{-4}$, obtained by adding the statistical and the systematic errors in quadrature, one obtains

$$0.22 \leq |C_7(m_b)| \leq 0.30. \tag{3}$$

This bound is subject to the residual next-to-leading order corrections. The inclusive branching ratio $\mathcal{B}(B \to X_s\gamma) = (2.32 \pm 0.67) \times 10^{-4}$ is consistent with the exclusive branching ratio $\mathcal{B}(B \to K^* + \gamma) = (4.5 \pm 1.0 \pm 0.9) \times 10^{-5}$, with $R(K^*/X_s) \equiv \Gamma(B \to K^* + \gamma)/\Gamma(B \to X_s + \gamma)$ calculated to be $0.1 \leq R(K^*/X_s) \leq 0.2$ in most theoretical models of recent vintage [3], [14]-[21].

The bound on $|C_7(m_b)|$ given in (3) can be used to constrain the non-SM contribution to the decay rate $\mathcal{B}(B \to X_s\gamma)$. The inclusive branching ratio in the SM, including the leading corrections in the anomalous dimension matrix and $O(\alpha_s)$ virtual and bremstrahlung corrections, has been estimated to be $\mathcal{B}(B \to X_s\gamma) = (2.8 \pm 1.0) \times 10^{-4}$ [3]. With $m_t = 174 \pm 16$ GeV determined from the CDF data [22], a good part of the uncertainty in the theoretical estimates of $\mathcal{B}(B \to X_s\gamma)$ is due to the scale dependence of the perturbative QCD framework and the QCD scale parameter entering α_S itself. Recently, parts of the next-to-leading-order corrections have been included in the anomalous dimension matrix and the resulting decay rate $\Gamma(B \to X_s + \gamma)$ has been recalculated [21]. The inclusion of these terms reduces the scale-dependence of the effective coefficient $C_7(\mu)$ as the scale μ is varied in the range $m_b/2 \leq \mu \leq 2m_b$. The partial next-to-leading-order, however, not unexpectedly shows a regularization scheme-dependence and its value is also somewhat diminished compared to the leading-log estimates. This reduces the branching ratio, and the (partial) next-to-leading-order estimates give $\mathcal{B}(B \to X_s\gamma) = (1.9 \pm 0.2 \pm 0.5) \times 10^{-4}$ [21]. The complete next-to-leading-order result is not yet available and hence the estimates of the SM for $\mathcal{B}(B \to X_s\gamma)$ are not completely quantitative, although the inclusive rate (1) and the SM estimates [3, 21] are in good agreement. The sensitivity to new physics in $B \to X_s\gamma$ is therefore somewhat entangled with the QCD corrections. Despite this, the CLEO data on rare B decays have provided valuable constraints on the parameters of models that are popular candidates for the extensions of the SM, and in some cases these constraints are very competitive compared to the ones following from direct and indirect searches [12].

The determination of $|C_7(m_b)|$ from the inclusive branching ratio $\mathcal{B}(B \to X_s\gamma)$ is a prototype of the kind of analysis that we would like to propose here to be carried out for the rare B decays in general and for the semileptonic decays $B \to X_s\ \ell^+\ell^-$, in particular. In the standard model, a measurement of the radiative rare B decay $B \to X_s\gamma$ mentioned above and related ones, such as $B \to X_s\ \ell^+\ell^-$, $B \to X_d\ \ell^+\ell^-$, the corresponding exclusive decays $B \to (K, K^*, \pi, \rho, ...)\ell^+\ell^-$, would lead to a determination of m_t and the CKM matrix element product $V_{ts}V_{tb}$ and $V_{td}V_{tb}$. The purely leptonic decays $B_s^0 \to \ell^+\ell^-$ and $B_d^0 \to \ell^+\ell^-$ and the modes $B_s^0 \to \gamma\gamma$, $B_d^0 \to \gamma\gamma$, while having very different final states and branching ratios – and hence representing experimentally very different propositions – have more or less the same information content in the SM as the decays mentioned above (see, for example, [23] and references cited therein).

The aim of this paper is to undertake first steps towards a model-independent analysis of the FCNC electroweak rare B decays. Although the method of analysing the data and the relevant theoretical framework being presented here are developed for the inclusive decays $B \to X_s\gamma$ and $B \to X_s + \ell^+\ell^-$, much of the general considerations being discussed apply also to the corresponding exclusive decays such as $B \to K^*\gamma$, $B \to K^*\ \ell^+\ell^-$ and $B \to$

$K\ell^+\ell^-$. Of course, the extraction of the short-distance physics in terms of the Wilson coefficients of the dominant operators from the data on exclusive decays would require the knowledge of the relevant form factors. This may compromise the precision on the short-distance part of the amplitudes in question at present, though advances in computational methods for QCD may allow quantitative conclusions to be drawn from exclusive decays also.

Our analysis is based on the renormalization group (RG)-improved treatment of the effective Hamiltonian relevant for B decays under consideration, obtained by integrating out the top quark and the other heavy degrees of freedom. The resulting Hamiltonian in the SM can be written as:

$$\mathcal{H}_{eff}(b \to sX) = -\frac{4G_F}{\sqrt{2}}\lambda_t \sum_{i=1}^{10} C_i(\mu)\mathcal{O}_i(\mu) \ . \tag{4}$$

Here X stands for $q\bar{q}$, γ, gluon and $\ell^+\ell^-$ and $\lambda_t = V_{ts}^* V_{tb}$; the operator basis contains dimension-5 and -6 operators and is given in the appendix.

The problem of carrying out a model-independent analysis in FCNC processes is evident from the SM expression for $\mathcal{H}_{eff}$ given above. In the most general case, which would also include Left-Right-symmetric (LR) models, the operator basis consists of 20 operators, having 20 independent coefficients C_i. However, as argued later, we shall limit the present analysis to left-handed fields only, in which case there are still 10 operators to be considered. The effective Hamiltonian then still involves 10 independent coefficients C_i and determining them experimentally is a monumental task. It is obvious that some theoretical assumptions have to be used to focus the attention on the more interesting Wilson coefficients. In our opinion, the promising coefficients from the stand-point of non-SM physics searches are the ones in which the electroweak loop effects (penguins and boxes in the diagrammatic language) play the dominant role.

The analysis carried out here is restricted to the models in which the effective Hamiltonian is of the form given in (4). We show later how measurements can be analysed to determine the inadequacy of this operator basis, should that happen. Although by no means completely general, the operator basis contained in $\mathcal{H}_{eff}$ encompasses most models of current theoretical interest, which include, apart from the SM, the 2HDM (both types I and II) and the MSSM. The effective Hamiltonian in the four-generation models, as well as in models with anomalous trilinear gauge and fermion couplings, can also be written in the above form.

The coefficients $C_i(M_W), i = 1, \ldots, 6$, determine the non-leptonic B-decay rates and the B-hadron lifetimes. Since data on B decays and the results obtained in the SM from (4), including QCD effects, are in good agreement with each other ($\pm 20\%$), there is not much room left for the first six coeffficients involving the four-quark operators to deviate from their SM values. So we fix $C_i(M_W), i = 1, \ldots, 6$, to their SM values. Beyond the leading-log approximation, these receive corrections of order $\alpha_s(M_W)$ at the large scale $\mu = M_W$; they should be incorporated in theoretical estimates

consistently with other higher-order effects. The coefficients of our interest are $C_7(\mu), ..., C_{10}(\mu)$, since they are generated at scale $\mu = M_W$ by electroweak loops (penguins and boxes). They govern the physics of the rare B decays $b \to s + g$, $B \to X_s\gamma$, $B \to X_s\ \ell^+\ell^-$ and $B_s^0 \to \ell^+\ell^-$. We shall concentrate on them and show how to extract these coefficients (both their signs and magnitudes) from data on radiative and (semi)leptonic rare B decays. These can be compared with the SM and extensions of it to search for new physics.

The experimental quantities we consider in this paper are the following:

- Inclusive radiative rare decay branching ratio $\mathcal{B}(B \to X_s\gamma)$;
- Invariant dilepton mass distributions $d\mathcal{B}(B \to X_s\ \ell^+\ell^-)/d\hat{s}$;
- Forward-backward (FB) charge asymmetry $\mathcal{A}(\hat{s})$ in $B \to X_s\ \ell^+\ell^-$.

The kinematic variables are defined as:

$$\begin{aligned} u &= (p_b - p_1)^2 - (p_b - p_2)^2, \\ s &= (p_1 + p_2)^2, \\ \hat{s} &= \frac{s}{m_b^2}, \\ w(s) &= \sqrt{(s - (m_b + m_s)^2)(s - (m_b - m_s)^2)}. \end{aligned} \tag{5}$$

where p_b, p_1 and p_2 denote, respectively, the momenta of the b quark ($= B$ hadron), ℓ^+ and ℓ^-. The FB asymmetry $\mathcal{A}(\hat{s})$ is defined with respect to the angular variable $z \equiv \cos\theta = u/w(s)$, where θ is the angle of the ℓ^+ with respect to the b-quark direction in the centre-of-mass system of the dilepton pair. It is obtained by integrating the doubly differential distribution $d^2\mathcal{B}/(dz\, d\hat{s})$ [24]:

$$\mathcal{A}(\hat{s}) \equiv \int_0^1 dz\, \frac{d^2\mathcal{B}}{dz\, d\hat{s}}(B \to X_s\ell^+\ell^-) - \int_{-1}^0 dz\, \frac{d^2\mathcal{B}}{dz\, d\hat{s}}(B \to X_s\ell^+\ell^-). \tag{6}$$

The rationale for concentrating on these measurements is the following. We remark that the decay rate $\mathcal{B}(B \to X_s\gamma)$ puts a bound on the absolute value of the coefficient $C_7(\mu)$. However, the radiative B decay rate by itself is not able to distinguish between the solutions $C_7(\mu) > 0$ (holding in the SM) and the solutions $C_7(\mu) < 0$, which, for example, are also allowed in the MSSM as one scans over the allowed parameter space. We recall that the invariant dilepton mass distribution and the forward-backward asymmetry in $B \to X_s\ \ell^+\ell^-$ are sensitive to the sign and magnitude of $C_7(\mu)$ [24, 25, 26]. This is easy to see in the approximation of neglecting the s-quark mass, in which limit the differential branching fraction for $B \to X_s\gamma$ can be written as:

$$\begin{aligned} \frac{d\mathcal{B}(B \to X_s\ \ell^+\ell^-)}{d\hat{s}} &= K(1-\hat{s})^2\{(|C_9^{eff}(\mu)|^2 + |C_{10}(\mu)|^2)(1+2\hat{s}) \\ &\quad + |C_7(\mu)|^2 \frac{4}{\hat{s}}(2+\hat{s}) + 12\ \mathrm{Re}\ (C_7(\mu)C_9^{eff}(\mu))\}, \end{aligned} \tag{7}$$

where K is a constant and $C_9^{eff}(\mu)$ is defined as

$$C_9^{eff}(\mu) = C_9(\mu) + Y(\mu, \hat{s}) \ , \tag{8}$$

where $Y(\mu, \hat{s})$ is a function involving the coefficients $C_i(\mu); i = 1, \ldots, 6$, and it depends on the kinematic variable $\hat{s}$ through the one-loop matrix element of the four-quark operators. Long-distance effects would also be contained in $Y(\mu, \hat{s})$; however, we shall not consider these here.

Consistent with our assumptions, we shall take the function $Y(\mu)$ from the SM and admit non-SM contributions only in $C_7(\mu)$, $C_8(\mu)$. $C_9(\mu)$, and C_{10}. From the above expression it is obvious that the dilepton invariant-mass distribution is sensitive to the real part of the product $C_7(\mu)C_9^{eff}(\mu)$ in sign and magnitude. However, this distribution by itself cannot determine the sign of C_9^{eff} and C_{10}. As the FB asymmetry and the dilepton rate are in general independent quantities, they provide independent constraints on the Wilson coefficients, and we argue that the FB asymmetry $\mathcal{A}(\hat{s})$ can be used to resolve these ambiguities. In the limit $m_s = 0$, the FB asymmetry has a simple form also:

$$\mathcal{A}(\hat{s}) = -\frac{3}{2} K (1-\hat{s})^2 C_{10}(\mu) \{ C_9^{eff}(\mu)\hat{s} + 4C_7(\mu) \}. \tag{9}$$

The $\hat{s}$-dependence in $\mathcal{A}(\hat{s})$ now allows us to disentangle the dependence on $C_7(\mu)$ and $C_9^{eff}(\mu)$. Moreover, the FB asymmetry $\mathcal{A}(\hat{s})$ is directly proportional to the coefficient $C_{10}(\mu)$ and hence the asymmetry is very effective in constraining $C_{10}(\mu)$.

The first measurements will be done for partially integrated dilepton mass distribution and asymmetry. We discuss how to extract the Wilson coefficients from these measurements. A given integrated branching ratio $\mathcal{B}(\Delta s)$ over a given range in s, Δs, and a given value of $C_7(\mu)$ can be analysed in terms of the contour plots drawn in the Wilson-coefficients plane $C_9(\mu)$ and $C_{10}(\mu)$. It is obvious from the quadratic equation (7) that, for a given $C_7(\mu)$, there is at most a four-fold ambiguity in the signs of $C_9(\mu)$ and $C_{10}(\mu)$. In addition one may make use of the integrated FB asymmetry $\mathcal{A}(\Delta s)$. For a fixed value of $\mathcal{A}(\Delta s)$ one finds hyperbolae in the C_9-C_{10} plane, for given sign and magnitude of $C_7(\mu)$. The intersection of the contours obtained from $\mathcal{B}(B \to X_s \ \ell^+\ell^-;\ \Delta s)$ and $\mathcal{A}(\Delta s)$ then determines the signs and magnitudes of all three Wilson coefficients $C_7(\mu), C_9(\mu)$ and $C_{10}(\mu)$. We plot, in the $C_9(\mu)$-$C_{10}(\mu)$ plane, the contours that are allowed from the solutions of the two algebraic equations for $\mathcal{B}(\Delta s)$ and $\mathcal{A}(\Delta s)$ for the two values of C_7, $C_7 = \pm 0.3$, and two invariant-mass intervals below the J/ψ and above the ψ' mass (see figs. 1-4), pointing out the SM solution and the general solutions in non-SM cases. It is, however, conceivable that there is no consistent solution of the two algebraic equations for $\mathcal{B}(\Delta s)$ and $\mathcal{A}(\Delta s)$ in $B \to X_s \ell^+\ell^-$ and the branching ratio $B \to X_s\gamma$ in terms of the coefficients $C_7(\mu)$, $C_9(\mu)$ and $C_{10}(\mu)$, which would then indicate that the operator basis chosen in describing the $\mathcal{H}_{eff}$ given above is incomplete. The LR-symmetric models, which

we have dropped from our discussion, is a case in point. Of course, given enough statistics the two distributions could be used to determine the coefficients from the data fits and compared with the values in the various models directly. We illustrate these analysis techniques for some assumed values of the branching ratios and asymmetry and representative values in the allowed parameter space in various models in terms of both the contour plots in the Wilson coefficient space and the distributions themselves.

This paper is organized as follows. In section 2, we briefly review the kinematics of the decays $B \to X_s\gamma$ and $B \to X_s\ \ell^+\ell^-$, define the amplitudes and the various distributions of interest. In section 3, we perform a numerical study of the differential and integrated branching ratio in $B \to X_s\ \ell^+\ell^-$. To illustrate the method, we have taken a representative value for the effective Wilson coefficient, $C_7(m_b) = \pm 0.3$, which lies within the presently allowed range for this quantity from data on $B \to X_s\gamma$. We give the partially integrated branching ratio $\mathcal{B}(\Delta s)$ and the asymmetry $\mathcal{A}(\Delta s)$, making the dependence on the coefficients C_9 and C_{10} explicit. The resulting constraints on these coefficients from the "low-dilepton mass" and "high-dilepton mass" regions are then displayed as contour plots in the C_9-C_{10} plane for some illustrative values of the branching ratios and FB asymmetries. The invariant dilepton mass spectrum in $B \to X_s\ \ell^+\ell^-$ and the FB asymmetry are also shown here for some representative values of the Wilson coefficients. In section 4 we discuss the predictions of specific models, namely the 2HDM (type I and type II) and the MSSM. These models allow a calculation of the coefficients $C_7(\mu), C_9(\mu)$ and $C_{10}(\mu)$ as a function of the model parameters. For the case of the 2HDM we show $C_7(\mu), C_9(\mu)$ and $C_{10}(\mu)$ as a function of the charged Higgs mass m_{H^+} for representative values of the ratio of the two vacuum expectation values v_2/v_1. As already noted [25], the type-I 2HDMs admit negative $C_7(\mu)$ solutions, as opposed to the positive $C_7(\mu)$ solution obtained in the SM. However, for the type-I models the negative $C_7(\mu)$ solutions are excluded by present data, as will be shown in section 4. To analyse the MSSM we vary the parameters of the model over the experimentally allowed values, and the resulting region in the $C_9(\mu)$–$C_{10}(\mu)$ plane is shown. In doing this, we have imposed the constraints on the coefficient $C_7(\mu)$ as explained earlier. The restrictions on the supersymmetric (SUSY) particle masses from present searches and the anticipated reach of experiments at the Tevatron and LEP-II are also imposed. The most interesting part of this exercise is that these constraints do allow both the negative and positive $C_7(\mu)$ solutions, which are consistent with the data on $B \to X_s\gamma$ but admit values of the coefficients $C_9(\mu)$ and $C_{10}(\mu)$ sufficiently different from those of the SM, thereby yielding very different differential distributions in the decay $B \to X_s\ \ell^+\ell^-$. These distributions are shown for some representative values of the Wilson coefficients. Section 5 contains a summary. To fix our notation we collect the relevant formulae for the effective Hamiltonian, including the RG-improved Wilson coefficients $C_i(\mu)$ in an appendix.

2 Estimates of $\mathcal{B}(B \to X_s\gamma)$, Invariant Dilepton Mass Distribution and Forward–Backward Asymmetry in $B \to X_s\ \ell^+\ell^-$

In the following we shall consider the inclusive decays $B \to X_s\gamma$ and $B \to X_s\ell^+\ell^-$, where ℓ is either electron or muon. It has been shown that inclusive B decays may be treated in a $1/m_b$ expansion, the leading term of which is the free quark decay. The next-to-laeding effects are of second order in $1/m_b$, i.e. $O(m_s^2/m_b^2)$ [27, 28, 29]. This is true for total rates, for partially integrated rates, and also for decay distributions, as long as one is not too close to the kinematic endpoint in which the energy release in the hadronic subprocess becomes small.

We shall also not include QCD corrections to the free-quark decay distributions, aside from the leading logarithms, which are induced by the renormalization group running. It is known that the measured inclusive lepton energy distributions of the charged-current-induced semileptonic transitions are well approximated by the partonic distributions $b \to (c,u)\ell^-\bar{\nu}_\ell$, including QCD corrections [31, 32]. We expect this for the flavour-changing neutral current semileptonic transitions as well.

The second proviso is that we shall concentrate on the short-distance contributions to the decays $B \to X_s\gamma$ and $B \to X_s\ \ell^+\ell^-$. This again is not a drastic oversimplification, as it is known that the long-distance contributions to the decay $B \to X_s\gamma$ are small [33, 34, 35] and those in the decays $B \to X_s\ \ell^+\ell^-$ are dominantly present at and near the J/ψ and ψ' poles, extending also to the region between them. These contributions can be modelled using data on the decays $B \to (J/\psi, \psi')X_s \to (\ell^+\ell^-)X_s$, which already exist and which are expected to become quite precise in the future. We shall thus concentrate on the distributions in the regions away from the resonances and consider the two regions

$$\begin{aligned} \text{“Low dilepton-mass”:} \qquad & 4m_\ell^2 \ \leq\ s \leq m_{J/\psi}^2 - \delta\ , \\ \text{“High dilepton-mass”:} \qquad & m_{\psi'}^2 + \delta \ \leq\ s \leq s_{max}, \end{aligned} \tag{10}$$

where δ is a cut-off that can be matched with the experimental cuts used in the analysis. In these two regions we expect only small long-distance effects. Due to limitations in rates and dilepton trigger requirements, we anticipate that the “Low dilepton-mass region” is accessible to e^+e^- experiments (CLEO and B factories) and the “High dilepton-mass region” typically to B experiments which will be carried out with hadron beams (CDF, HERA-B, LHC). Given high enough luminosity, this region can also be probed at the B factories.

2.1 Decay rate for $B \to X_s\gamma$

The procedure for the computation of the Wilson coefficients in the SM and extensions of it is by now standard. They are obtained at a large scale $\mu^2 = M_W^2$ (in general at $\mu^2 = m_Y^2$, where m_Y stands generically for the mass of the heavy degrees of freedom) by integrating out degrees of freedom heavier than μ [36], and are sensitive to the presence of new physics. Then the renormalization group (RG) equations are used to scale down these coefficients to the scale that is typical for B-hadron decays, namely $\mu = O(m_b)$. In this way large logarithms of the form $\alpha_s \ln M_W^2$ are shifted from the matrix element into the Wilson coefficients. The RG evolution of the Wilson coefficients $C_i(\mu)$ involves the (10×10) anomalous dimension matrix, which has now been calculated at the one-loop level [37, 38]. This matrix and the solutions of the RG equations in terms of the effective coefficients $C_i(\mu)$ are given in the appendix.

Starting from the effective Hamiltonian as given in the appendix, one finds that only one operator, namely $\mathcal{O}_7$ contributes at tree level. The contribution of the QCD bremsstrahlung process $b \to s\gamma + g$ and the virtual corrections to $b \to s\gamma$ have been calculated in $O(\alpha\alpha_s)$ in ref. [30]. Expressed in terms of the inclusive semileptonic branching ratio $BR(B \to X\ell\nu_\ell)$, one can express the branching ratio $\mathcal{B}(B \to X_s\gamma)$ as:

$$\mathcal{B}(B \to X_s\gamma) = 6\frac{\alpha}{\pi}\frac{|\lambda_t|^2}{|V_{cb}|^2}\frac{|C_7(\mu)|^2 K(\mu)}{f(m_c/m_b)[1-(2\alpha_s)/(3\pi)h(m_c/m_b)]} \times \mathcal{B}_{sl} \ , \quad (11)$$

where

$$f(r) = 1 - 8r^2 + 8r^6 - r^8 - 24r^4\ln(r)$$

is the phase-space function for $\Gamma(b \to c + \ell\nu_\ell)$ and $\mathcal{B}_{sl} = 10.5\%$ is the semileptonic branching fraction. The function $h(r)$ accounts for QCD corrections to the semileptonic decay and can be found, for example, in ref. [31]. It is a slowly varying function of r and, for a typical quark-mass ratio of $r = 0.35 \pm 0.05$, it has the value $h(r) = 2.37 \mp 0.13$. The contributions from the decays $b \to u\ \ell\ \nu_\ell$ have been neglected in the denominator in (11) since they are numerically inessential because $|V_{ub}| \ll |V_{cb}|$.

The inclusive decay width for $B \to X_s\gamma$ is dominantly contributed by the magnetic-moment operator $\mathcal{O}_7$, hence the rationale of factoring out its coefficient in the expression for $\mathcal{B}(B \to X_s\gamma)$ in Eq. (11). Including $O(\alpha_s)$ corrections brings to the fore other operators with their specific Wilson coefficients. The effect of these additional terms can be expressed in terms of the function $K(\mu)$, which lumps together the effects of bremsstrahlung corrections in the inclusive decay rate. The function $K(\mu)$ has been computed in the SM in [3] taking into account the dominant corrections from C_2 and C_8 (the coefficients of other operators are considerably smaller). Typically, $0.79 \le K(\mu) \le 0.86$ for $m_b/2 \le \mu \le 2m_b$. Since $C_8(\mu)$ receives possible non-SM contributions in the same way as $C_7(\mu)$, one should compute the K-factor and incorporate these corrections into a full next-to-leading-order

analysis. However, we are not working beyond leading order in this paper and so we ignore the K factor. Using the CLEO inclusive measurement

$$\mathcal{B}(B \to X_s\gamma) = (2.31 \pm 0.67) \times 10^{-4}, \tag{12}$$

we get the following bound on $C_7(\mu)$:

$$0.22 \leq |C_7(\mu)| \leq 0.30. \tag{13}$$

Using, however, the 90%-confidence-level range from the CLEO measurement $\mathcal{B}(B \to X_s\gamma) = (2.31 \pm 1.1) \times 10^{-4}$ and the theoretical calculation for $\mathcal{B}(B \to X_s\gamma)$ from [3] we obtain

$$0.19 \leq |C_7(\mu)| \leq 0.32. \tag{14}$$

This range, in our opinion, adequately reflects the present uncertainties. When not stated otherwise, we shall fix $|C_7(\mu)| = 0.3$, which is in comfortable agreement with the CLEO data.

2.2 Decay distributions in $B \to X_s\ \ell^+\ell^-$

Using $\mathcal{H}_{eff}$ given in (4), one obtains for the dilepton invariant mass distribution

$$\begin{aligned}\frac{d\mathcal{B}}{d\hat{s}} &= \mathcal{B}_{sl}\frac{\alpha^2}{4\pi^2}\frac{\lambda_t}{|V_{cb}|}^2\frac{1}{f(m_c/m_b)}\hat{w}(\hat{s})\Big[\left(|C_9 + Y(\hat{s})|^2 + C_{10}^2\right)\alpha_1(\hat{s},\hat{m}_s) \\ &\quad + \frac{4}{\hat{s}}C_7^2\alpha_2(\hat{s},\hat{m}_s) + 12\alpha_3(\hat{s},\hat{m}_s)C_7(C_9 + \text{ Re } Y(s))\Big],\end{aligned} \tag{15}$$

where the auxiliary functions are defined as follows:

$$\alpha_1(\hat{s},\hat{m}_s) = -2\hat{s}^2 + \hat{s}(1+\hat{m}_s^2) + (1-\hat{m}_s^2)^2 \tag{16}$$

$$\alpha_2(\hat{s},\hat{m}_s) = -(1+\hat{m}_s^2)\hat{s}^2 - (1+14\hat{m}_s^2+\hat{m}_s^4)\hat{s} + 2(1+\hat{m}_s^2)(1-\hat{m}_s^2)^2 \tag{17}$$

$$\alpha_3(\hat{s},\hat{m}_s) = (1-\hat{m}_s^2)^2 - (1+\hat{m}_s^2)\hat{s} \tag{18}$$

$$\begin{aligned}Y(\hat{s}) &= g(m_c/m_b,\hat{s})(3C_1 + C_2 + 3C_3 + C_4 + 3C_5 + C_6) \\ &\quad -\frac{1}{2}g(1,\hat{s})(4C_3 + 4C_4 + 3C_5 + C_6) \\ &\quad -\frac{1}{2}g(0,\hat{s})(C_3 + 3C_4) + \Delta C_9\end{aligned} \tag{19}$$

and $g(z,\hat{s})$ is the one-loop function given in the appendix. Furthermore, the constant ΔC_9 depends on the scheme, which is chosen in the evaluation of the one-loop matrix elements of the operators $\mathcal{O}_1 \cdots \mathcal{O}_6$. It contains also a large logarithm $\ln(M_W^2/m_b^2)$, which is not due to QCD effets but rather

comes from the one-loop matrix elements of $\mathcal{O}_1 \cdots \mathcal{O}_6$. In the $\overline{\rm MS}$ scheme one obtains [25]

$$\Delta C_9 = \frac{4\pi}{\alpha_s(M_W)} \left\{ \frac{4}{33} \left[1 - \left(\frac{\alpha_s(M_W)}{\alpha_s(m_b)} \right)^{-11/23} \right] - \frac{8}{87} \left[1 - \left(\frac{\alpha_s(M_W)}{\alpha_s(m_b)} \right)^{-29/23} \right] \right\}, \tag{20}$$

which generates the correct logarithms in the limit $\alpha_s \to 0$.

The corresponding differential asymmetry as defined in (6) is

$$\mathcal{A}(\hat{s}) \;=\; -\mathcal{B}_{sl} \frac{3\alpha^2}{8\pi^2} \frac{1}{f(m_c/m_b)} \hat{w}^2(\hat{s}) C_{10} \left[\hat{s}(C_9 + \ \mathrm{Re}\ Y(\hat{s})) + 4C_7(1 + \hat{m}_s^2/\hat{s}) \right] \tag{21}$$

In the subsequent section, we shall be evaluating the partial branching ratio $\mathcal{B}(\Delta s)$ and partial FB asymmetry $\mathcal{A}(\Delta s)$, where Δs defines an interval in the dilepton invariant mass. All numerical calculations are done with a non-zero value for the s-quark mass, $m_s = 500$ MeV. The asymmetry in the dilepton angular distribution in the SM can be qualitatively understood as follows. The decays $B \to X_s\ \ell^+\ell^-$ occur through γ , Z and W^+W^- exchange diagrams. For small m_t ($m_t/M_W \ll 1$) the photon contribution dominates and the vector-like interactions to the leptonic current remain substantial; consequently, the asymmetry is small. However, for $m_t/M_W \geq 2$, as suggested by the CDF value for m_t, the contribution from the Z-exchange diagrams becomes important and the coefficient of the left-handed leptonic current grows as m_t^2, leading to a large asymmetry.

3 Analysis of the Decays $B \to X_s\gamma$ and $B \to X_s\ell^+\ell^-$

In this section we shall discuss how the Wilson coefficients appearing in the effective Hamiltonian may be extracted from the experimental information. We shall assume that all the matrix elements are normalized at the scale $\mu \sim m_b$, the mass of the b quark and hence the decay distributions are given in terms of the Wilson coefficients at the scale m_b. The SM makes specific predictions for these coefficients (modulo perturbative QCD uncertainties), but if there is physics beyond the SM, these coefficients will in general be modified.

We will somewhat elaborate on this point. A specific model provides the set of Wilson coefficients at high scales, which we shall choose to be the scale of the weak bosons $\mu = M_W$. Furthermore, we shall integrate out heavy degrees of freedom at the same scale $\mu = M_W$; this procedure introduces an uncertainty due to the difference in the masses of the heavy degrees of freedom, as for example arising from $m_t \simeq 2M_W$. However, since the QCD coupling constant is small at these very high scales and does not appreciably change between these thresholds, it is a reasonably accurate approximation to

neglect QCD corrections for scales above $\mu = M_W$. Starting from this scale, the Wilson coefficients are obtained from the solution of the renormalization group equations at the scale $\mu \sim m_b$, where we use the one-loop result for the anomalous dimensions and the beta function (see appendix).

In order to determine the sign of C_7 and the other two coefficients C_9 and C_{10}, one has to study the decay distributions and rates in $B \to X_s \ell^+ \ell^-$, where ℓ is either electron or muon. As already discussed, these decays are sensitive to the sign of C_7, and to C_9 and C_{10}. The first experimental information available in the decay $B \to X_s \ell^+ \ell^-$ will be a measurement of the branching fraction in a certain kinematic region of the invariant mass s of the lepton pair. In order to minimize long-distance effects we shall consider the kinematic regime for s below the J/ψ mass (low invariant mass) and for s above the mass of the ψ' (high invariant mass). Integrating (20) over these regions for the invariant mass one finds[3]

$$\mathcal{B}(\Delta s) = A(\Delta s)\left(C_9^2 + C_{10}^2\right) + B(\Delta s) C_9 + C(\Delta s), \tag{22}$$

where A, B and C are fixed in terms of the Wilson coefficients $C_1 \cdots C_6$ and C_7. We derive from (15):

$$A(\Delta s) = \mathcal{B}_{sl} \frac{\alpha^2}{4\pi^2} \frac{1}{f(m_c/m_b)} \int_{\Delta s} d\hat{s}\, \hat{u}(\hat{s}) \alpha_1(\hat{s}, \hat{m}_s) \tag{23}$$

$$B(\Delta s) = \mathcal{B}_{sl} \frac{\alpha^2}{4\pi^2} \frac{1}{f(m_c/m_b)} \int_{\Delta s} d\hat{s}\, \hat{u}(\hat{s}) \left[2\alpha_1(\hat{s}, \hat{m}_s)\ \mathrm{Re}\ Y(\hat{s}) + 12 C_7 \alpha_3(\hat{s}, \hat{m}_s)\right] \tag{24}$$

$$\begin{aligned} C(\Delta s) = \mathcal{B}_{sl} \frac{\alpha^2}{4\pi^2} \frac{1}{f(m_c/m_b)} \int_{\Delta s} d\hat{s}\, \hat{u}(\hat{s}) \Big[& \alpha_1(s, \hat{m}_s) \left\{ (\ \mathrm{Re}\ Y(\hat{s}))^2 + (\ \mathrm{Im}\ Y(\hat{s}))^2 \right\} \\ & + \frac{4}{s} |C_7|^2 \alpha_2(s, \hat{m}_s) + 12 \alpha_3(s, \hat{m}_s) C_7\ \mathrm{Re}\ Y(\hat{s}) \Big], \end{aligned} \tag{25}$$

where the auxiliary functions α_i, $i = 1, 2, 3$, are as given above.

In our analysis we keep the values for $C_1 \cdots C_6$ and the modulus of C_7 fixed and hence $A(\Delta s)$, $B(\Delta s)$ and $C(\Delta s)$ may be calculated for the two invariant-mass ranges of interest. For the numerical analysis we use $m_b = 4.7$ GeV, $m_c = 1.5$ GeV, $m_s = 0.5$ GeV. The values for the Wilson coefficients $C_1, \ldots, C_6$ are given in the appendix. The resulting coefficients A, B, and C are listed in Table 1.

Inspection of (25) shows that the integrand for $C(\Delta s)$ behaves as $1/s$ for small values of s, leading to a logarithmic dependence of $C(\Delta s)$ on the lepton mass for the case of the low invariant mass region. In fact, this is the only

[3] In performing the integrations over Δs we have set the resolution parameter δ to zero, since we do not consider any long-distance contribution. The long-distance contribution peaks strongly at the J/ψ and ψ' and δ has to be several times the width of these resonances in order to avoid large long-distance effects. However, calculating only the short-distance part one may safely neglect δ, since the short-distance contribution is flat in this region.

Δs	C_7	$A(\Delta s)/10^{-8}$	$B(\Delta s)/10^{-8}$	$C(\Delta s)/10^{-8}$ $\ell = e$	$C(\Delta s)/10^{-8}$ $\ell = \mu$
$4m_\ell^2 < s < m_{J/\psi}^2$	$+0.3$	2.86	-5.76	84.1	76.6
$4m_\ell^2 < s < m_{J/\psi}^2$	-0.3	2.86	-20.8	124	116
$m_{\psi'}^2 < s < (1 - m_s^2)$	$+0.3$	0.224	-0.715	0.654	0.654
$m_{\psi'}^2 < s < (1 - m_s^2)$	-0.3	0.224	-1.34	2.32	2.32

Table 1: Values for the coefficients $A(\Delta s)$, $B(\Delta s)$ and $C(\Delta s)$ for the decay $B \to X_s \ell^+ \ell^-$.

point where the masses of the leptons enter our analysis, and from this one may obtain the corresponding coefficients for $\ell = \mu$:

$$C(4m_\mu^2 < s < m_{J/\psi}^2) = C(4m_e^2 < s < m_{J/\psi}^2) - 8|C_7|^2(1+\hat{m}_s^2)(1-\hat{m}_s^2)^3 \ln\left(\frac{m_\mu^2}{m_e^2}\right). \tag{26}$$

Of course one may apply (26) also to obtain C for any other lower cut s_0 on the lepton invariant mass, as long as $s_0 \ll m_{J/\psi}^2$.

For a measured branching fraction $\mathcal{B}(\Delta s)$, one can solve the above equation for $\mathcal{B}(\Delta s)$, obtaining concentric circles in the C_9-C_{10} plane, with their centre lying at $C_9^* = B(\Delta s)/(2A(\Delta s))$ and $C_{10}^* = 0$. The radius R of these circles is proportional to

$$R = \sqrt{\mathcal{B}(\Delta s) - \mathcal{B}_{min}(\Delta s)}, \tag{27}$$

where the minimum branching fraction

$$\mathcal{B}_{min}(\Delta s) = C(\Delta s) - \frac{B^2(\Delta s)}{4A(\Delta s)} \tag{28}$$

is determined mainly by the present data on $B \to X_s\gamma$, i.e. by $|C_7|$. For the cases of interest one obtains, with the help of Table 1:

$$\mathcal{B}_{min}(4m_e^2 < s < m_{J/\psi}^2) = \begin{cases} 8.1 \times 10^{-7} \text{ for } C_7 = 0.3 \\ 8.6 \times 10^{-7} \text{ for } C_7 = -0.3, \end{cases} \tag{29}$$

$$\mathcal{B}_{min}(m_{\psi'}^2 < s < (1 - m_s^2)) = \begin{cases} 8.5 \times 10^{-10} \text{ for } C_7 = 0.3 \\ 3.0 \times 10^{-9} \text{ for } C_7 = -0.3. \end{cases} \tag{30}$$

Note that $\mathcal{B}(\Delta s)$ is an even function of C_{10}, so one is not able to fix the sign of C_{10} from a measurement of $\mathcal{B}(\Delta s)$ alone.

To further pin down the Wilson coefficients, one could perform a measurement of the forward-backward asymmetry $\mathcal{A}$, which has been defined above. The asymmetry is an odd function of C_{10}, and for a fixed value of the total branching ratio in this kinematic region one obtains, from integrating

Δs	C_7	$\alpha(\Delta s)/10^{-9}$	$\beta(\Delta s)/10^{-9}$
$4m_\ell^2 < s < m_{J/\psi}^2$	$+0.3$	-6.08	-24.0
$4m_\ell^2 < s < m_{J/\psi}^2$	-0.3	-6.08	55.4
$m_{\psi'}^2 < s < (1-m_s^2)$	$+0.3$	-0.391	0.276
$m_{\psi'}^2 < s < (1-m_s^2)$	-0.3	-0.391	1.37

Table 2: Values for the coefficients $\alpha(\Delta s)$and $\beta(\Delta s)$.

over a range (Δs):

$$\mathcal{A}(\Delta s) = C_{10}\left(\alpha(\Delta s)C_9 + \beta(\Delta s)\right), \tag{31}$$

where

$$\alpha(\Delta s) = -\mathcal{B}_{sl}\frac{3\alpha^2}{8\pi^2}\frac{1}{f(m_c/m_b)}\int_{\Delta s} d\hat{s}\,\hat{u}^2(\hat{s})\hat{s} \tag{32}$$

$$\beta(\Delta s) = -\mathcal{B}_{sl}\frac{3\alpha^2}{8\pi^2}\frac{1}{f(m_c/m_b)}\int_{\hat{s}} d\hat{s}\,\hat{u}^2(\hat{s})\left[\hat{s}\ \mathrm{Re}\ Y(\hat{s}) + 4C_7(1+\hat{m}_s^2)\right] \tag{33}$$

For a fixed value of $\mathcal{A}(\Delta s)$, one obtains hyperbolic curves in the C_9-C_{10} plane; like the coefficients A, B and C, the parameters α and β are given in terms of the Wilson coefficients $C_1 \cdots C_6$ and C_7, and the kinematic region of s considered; their values are presented in Table 2.

Given the two experimental inputs, the branching fraction $\mathcal{B}(\Delta s)$ and the corresponding asymmetry $\mathcal{A}(\Delta s)$, one obtains a fourth-order equation for the Wilson coefficients C_9 and C_{10}, which admits in general four solutions. In figs. 1-4 we plot the contours for a fixed value for the branching fraction $\mathcal{B}(\Delta s)$ and the FB asymmetry $\mathcal{A}(\Delta s)$. Since $\mathcal{B}(\Delta s)$ is an even function of C_{10} and $\mathcal{A}(\Delta s)$ is an odd one, we only plot positive values for C_{10}. The asymmetry vanishes for $C_{10} = 0$, but also for $C_9 = -\beta(\Delta s)/\alpha(\Delta s)$. The two lines $C_{10} = 0$ and $C_9 = -\beta(\Delta s)/\alpha(\Delta s)$ divide the C_9-C_{10} plane into four quadrants, in which the asymmetry has a definite sign. Reflecting the hyperbolae on the line $C_{10} = 0$ or $C_9 = -\beta(\Delta s)/\alpha(\Delta s)$ results in a sign change of the asymmetry.

Figures 1 and 2 show the contours in the $C_9(\mu)$-$C_{10}(\mu)$ plane for the low-invariant-mass region $4m_e^2 < s < m_{J/\psi}^2$, and figs. 3 and 4 are for the high-invariant-mass region $m_{\psi'}^2 < s < (1-\hat{m}_s)^2$. Figures 1 and 3 are obtained for $C_7(\mu) = 0.3$, while figs. 2 and 4 are for $C_7(\mu) = -0.3$. The possible solutions for C_9 and C_{10} are given by the intersections of the circle corresponding to the measured branching fraction and the hyperbola, corresponding to the measured asymmetry. Assuming the SM values for both $\mathcal{B}(\Delta s)$ and $\mathcal{A}(\Delta s)$, one obtains the solid lines in figs. 1-4. The possible solutions in this case

are represented by solid dots (SM solutions) and solid squares (other non-SM possible solutions).

From the figures one reads off that for the SM values of $\mathcal{B}$ and $\mathcal{A}$ one has more than one solution for the coefficients C_9 and C_{10}, but the ambiguity may in general be resolved by measuring both the low and the high invariant mass regions.

However, there is in principle also the possibility that the equations do not have a solution for C_9 and C_{10}. This is the case, for example, when the asymmetry is large and the branching fraction small, in which case the hyperbola may not intersect with the corresponding circle any more. If this happens one has to conclude that the present analysis is not complete; in other words, the operator basis we started from is not complete and physics beyond the SM will be present in the form of additional operators such as right-handed currents.

The upper and lower limits for the asymmetry as a function of the branching fraction may be obtained analytically and are given by

$$\mathcal{A}(\Delta s)_\pm = \bar{R}\cos\theta_\pm \left(\alpha(\Delta s)\bar{R}\sin\theta_\pm + y\right), \tag{34}$$

with

$$\bar{R} = \sqrt{\frac{\mathcal{B}(\Delta s) - \mathcal{B}_{min}(\Delta s)}{A(\Delta s)}} \tag{35}$$

$$\sin\theta_\pm = \frac{1}{4}\left[-\frac{y}{\alpha(\Delta s)\bar{R}} \mp \sqrt{\frac{y^2}{\alpha^2(\Delta s)\bar{R}^2} + 8}\right] \tag{36}$$

$$y = \beta(\Delta s) - \frac{B(\Delta s)\alpha(\Delta s)}{2A(\Delta s)}. \tag{37}$$

These boundaries are shown in fig. 5 for the low- and the high-invariant-mass region respectively. From these figures it is obvious that the bound is in fact non-trivial: it lies in any case far below the bound $|\mathcal{A}| < \mathcal{B}$.

If data become more precise one may in fact also expect a measurement of the spectrum and the asymmetry as a function of s. The spectrum itself is very sensitive to the values of the Wilson coefficients and to the sign of C_7. In fig. 6 we plot the various contributions to the spectrum, for positive and for negative C_7.

In a similar way, it may become possible to measure also the differential asymmetry

$$\mathcal{A}(s) = \int_{-1}^{0} dz\, \frac{d^2\mathcal{B}}{d\hat{s}dz} - \int_{0}^{1} dz\, \frac{d^2\mathcal{B}}{d\hat{s}dz}, \tag{38}$$

which is also sensitive to the sign of C_7. The various contributions to $\mathcal{A}(s)$ are shown in fig. 7.

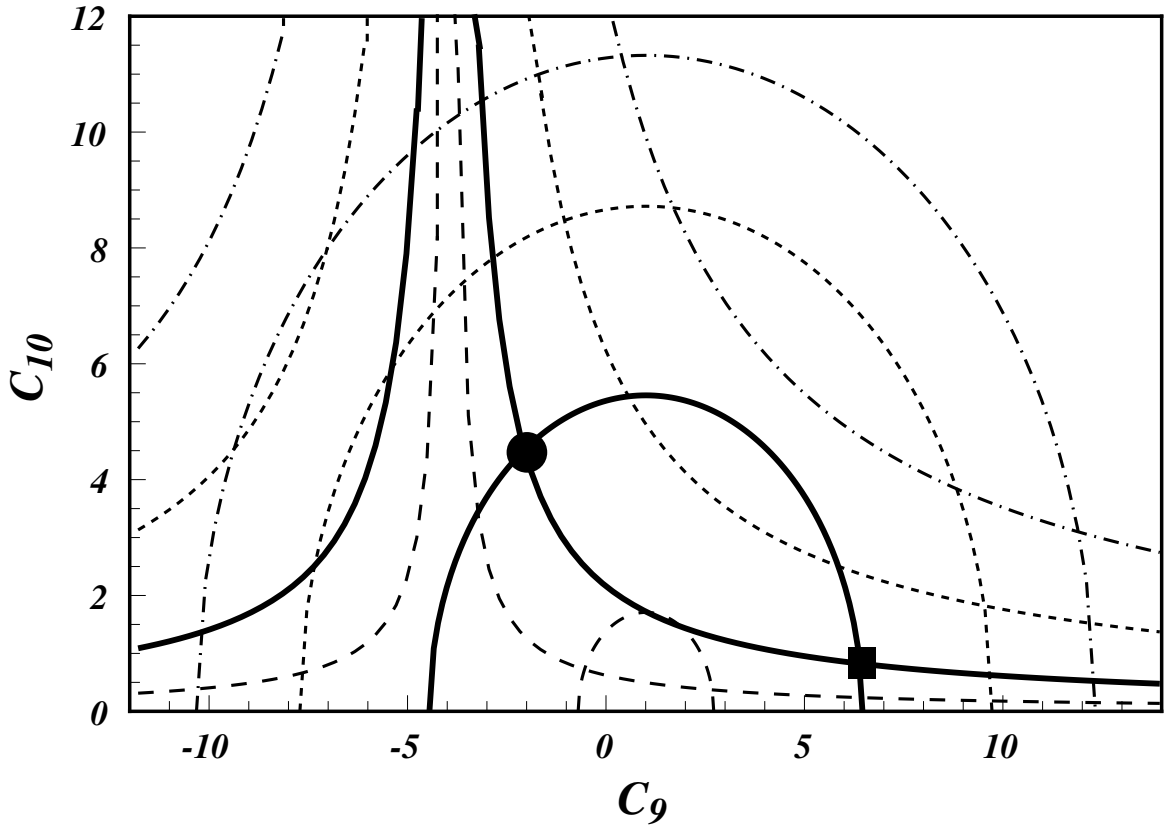

Figure 1: Contour plots of $\mathcal{B}(\Delta s)$ and $\mathcal{A}(\Delta s)$ in the C_9-C_{10} plane for the low-invariant-mass region $4m_\ell^2 < s < m_{J/\psi}^2$ and $C_7 = 0.3$. The circles correspond to fixed values of $\mathcal{B}$: $\mathcal{B} = 5.6 \times 10^{-6}$ (solid curve), $\mathcal{B} = 3.0 \times 10^{-6}$ (long-dashed curve), $\mathcal{B} = 1.0 \times 10^{-5}$ (short-dashed curve), $\mathcal{B} = 1.5 \times 10^{-5}$ (dash-dotted curve). The left branches of the hyperbolae correspond to positive values of $\mathcal{A}$: $\mathcal{A} = 1.7 \times 10^{-7}$ (solid curve), $\mathcal{A} = 5.0 \times 10^{-8}$ (long-dashed curve), $\mathcal{A} = 5.0 \times 10^{-7}$ (short-dashed curve), $\mathcal{A} = 1.0 \times 10^{-6}$ (dash-dotted curve). The right branches of the hyperbolae correspond to negative values of $\mathcal{A}$: $\mathcal{A} = -1.41 \cdot 10^{-8}$ (solid curve), $\mathcal{A} = -5.0 \cdot 10^{-9}$ (long-dashed curve), $\mathcal{A} = -3.0 \cdot 10^{-8}$ (short-dashed curve), $\mathcal{A} = -6.0 \cdot 10^{-8}$ (dash-dotted curve). For negative values of C_{10}, the figure is simply reflected with $\mathcal{A} \to -\mathcal{A}$. The solid dot indicates the SM values for C_9 and C_{10}. The solid square is another allowed solution resulting from the SM values of $\mathcal{B}$ and $\mathcal{A}$.

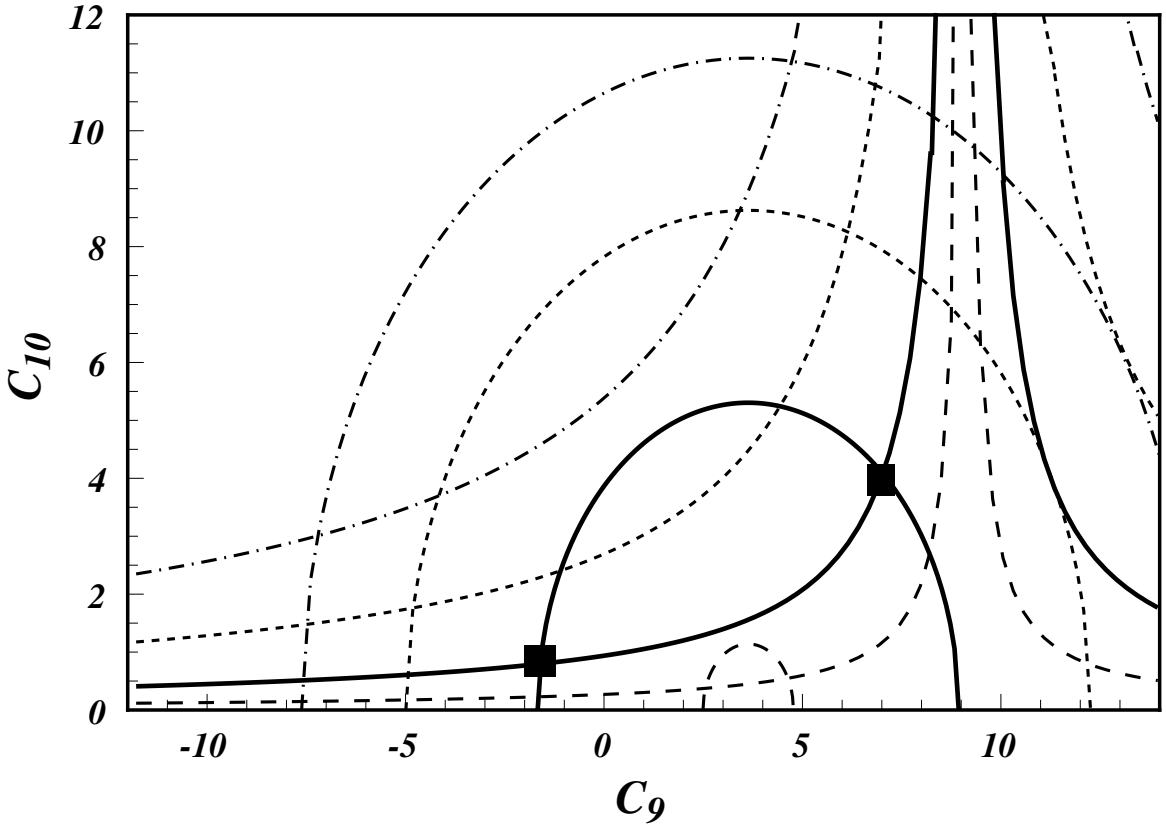

Figure 2: Same as in fig. 1, but for $C_7 = -0.3$.

4 Model Predictions for the Wilson Coefficients

Once the parameters C_7, C_9, and C_{10} have been extracted from experimental data, a direct comparison with different theoretical predictions can be made. If a deviation from the SM result is observed, new models accounting for this discrepancy, can be looked for. If no such deviation is observed, the result can be used to set bounds on new physics.

As already alluded to in the introduction, the operator basis considered here is not the most general one. For example, in the left-right symmetric (LR) models the basis (4) will have to be enlarged to incorporate the extended $SU(2)_L \times SU(2)_R \times U(1)$ gauge sector. The enlarged set contains the SM operators contained in $\mathcal{H}_{eff}$ above and another set of 10 operators obtained from this by flipping the chirality structure of the fermion fields $P_L \to P_R$, where $P_{L,R} = (1 \pm \gamma_5)/2$, increasing the number of independent Wilson coefficients to 20.

Since we are restricting the operator basis to exclude *ab initio* LR-symmetric models, we give reasons why such extensions of the SM are unlikely to make a significant contribution to rare B decays. In the minimal LR-symmetric models, the right-handed CKM matrix is identical to, or the complex conjugate of, the left-handed CKM matrix. However, in this case, there are

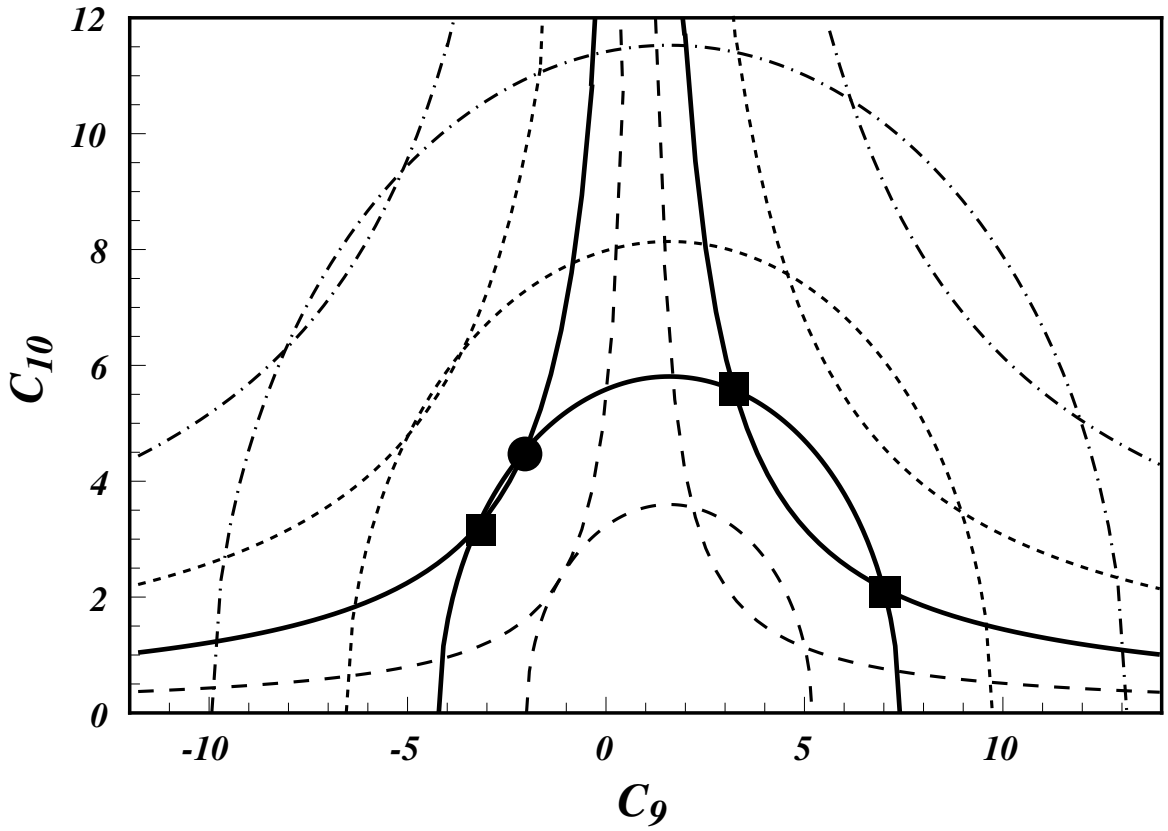

Figure 3: Contour plots of $\mathcal{B}(\Delta s)$ and $\mathcal{A}(\Delta s)$ in the C_9-C_{10} plane for the high-invariant-mass region $m_{\psi'}^2 < s < (1-m_s)^2$ and for $C_7 = 0.3$. The circles correspond to fixed values of $\mathcal{B}$: $\mathcal{B} = 2.56\times10^{-7}$ (solid curve), $\mathcal{B} = 1.0\times10^{-7}$ (long-dashed curve), $\mathcal{B} = 5.0\times10^{-7}$ (short-dashed curve), $\mathcal{B} = 1.0 \times 10^{-6}$ (dash-dotted curve). The left branches of the hyperbolae correspond to positive values of $\mathcal{A}$: $\mathcal{A} = 1.41 \times 10^{-8}$ (solid curve), $\mathcal{A} = 5.0 \times 10^{-9}$ (long-dashed curve), $\mathcal{A} = 3.0 \times 10^{-8}$ (short-dashed curve), $\mathcal{A} = 6.0 \times 10^{-8}$ (dash-dotted curve). The right branches of the hyperbolae correspond to negative values of $\mathcal{A}$: $\mathcal{A} = -1.41\times10^{-8}$ (solid curve), $\mathcal{A} = -5.0\times10^{-9}$ (long-dashed curve), $\mathcal{A} = -3.0\times10^{-8}$ (short-dashed curve), $\mathcal{A} = -6.0 \times 10^{-8}$ (dash-dotted curve). For negative values of C_{10}, the figure is simply reflected with $\mathcal{A} \to -\mathcal{A}$. The solid dot indicates the SM Values for C_9 and C_{10}. The solid squares are other allowed solutions resulting from the SM values of $\mathcal{B}$ and $\mathcal{A}$.

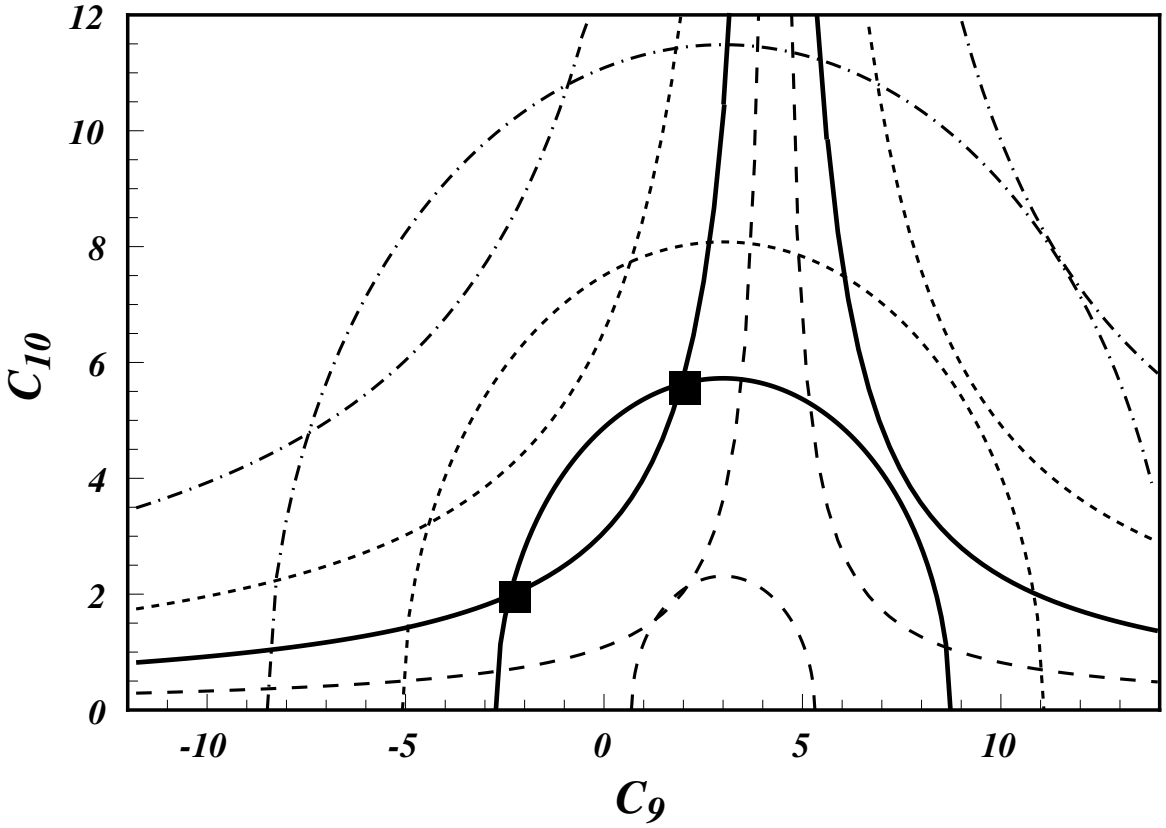

Figure 4: Same as in fig. 3, but for $C_7 = -0.3$.

rather strong lower limits on the mass of W_R, $M_R > 1.5 - 2.5$ TeV, arising from the condition that the short-distance contributions to the K_L–K_S mass difference not exceed the experimental value [39]. In view of this restriction on M_R, it would be difficult to see tangible differences between the SM and the minimal LR models in rare B decays, much as has been argued for the B^0–$\overline{B^0}$ mixing ratio x_s and x_d [40]. These qualitative anticipations have been borne out by explicit calculations [10, 11].

The situation with the non-minimal LR models is more involved [41]. While the bounds on m_R from Δm_K can be evaded, the constraints from ϵ_K force m_R to be in excess of 30 TeV, in general [42]. So, we shall no longer entertain the LR models, asserting that the present and impending constraints following from $\mathcal{B}(B \to X_s\gamma)$, x_d and Δm_K render the LR-symmetric-model effects in the FCNC semileptonic decays $B \to X_s\, \ell^+\ell^-$ insignificantly small and restrict the operator basis to the one given in (4). In this section, we consider as illustrative examples two popular extensions of the SM (the MSSM and the 2HDM) and study how the predictions for the Wilson coefficients C_7, C_9, and C_{10} are altered in these models, compared to the SM.

Supersymmetric models have a new source of flavour-changing neutral currents because of the quark-squark-gluino vertex, which is, in general, not diagonal in generation space [43]. If the generation mixings of such vertices were arbitrarily large, they would lead to phenomenologically unac-

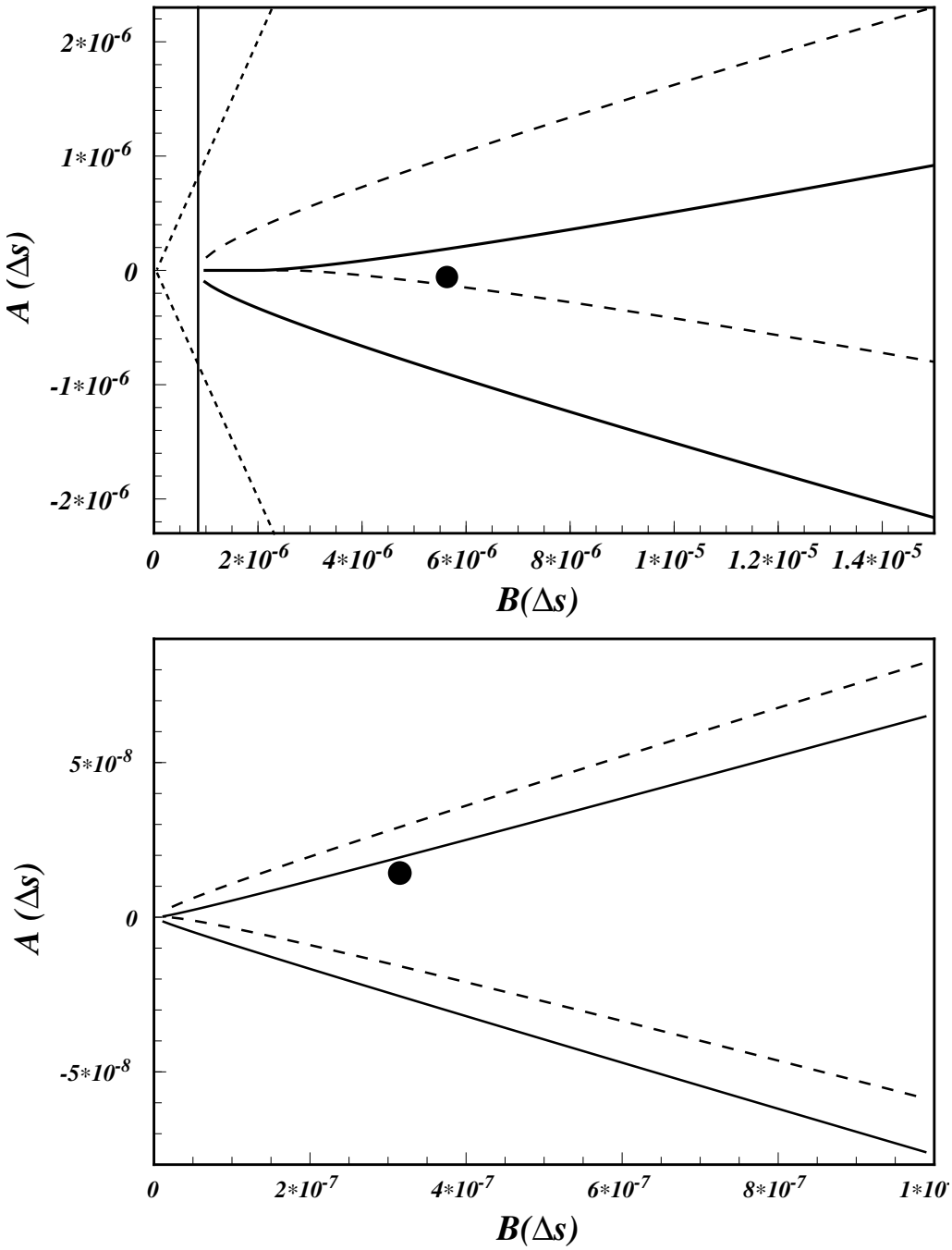

Figure 5: The bounds for the partially integrated asymmetry $\mathcal{A}(\Delta s)$ as a function of the partial dilepton branching ratio $\mathcal{B}(\Delta s)$. The upper plot is for the "low-invariant-mass region" and the lower one is for the "high-invariant-mass region" as defined in the text. The boundary demarcated by the solid curves are for the positive value $C_7 = 0.3$, the long-dashed curves correspond to the negative value $C_7 = -0.3$. The dotted line is the trivial bound $|\mathcal{A}| < \mathcal{B}$. The solid dot denotes the SM value.

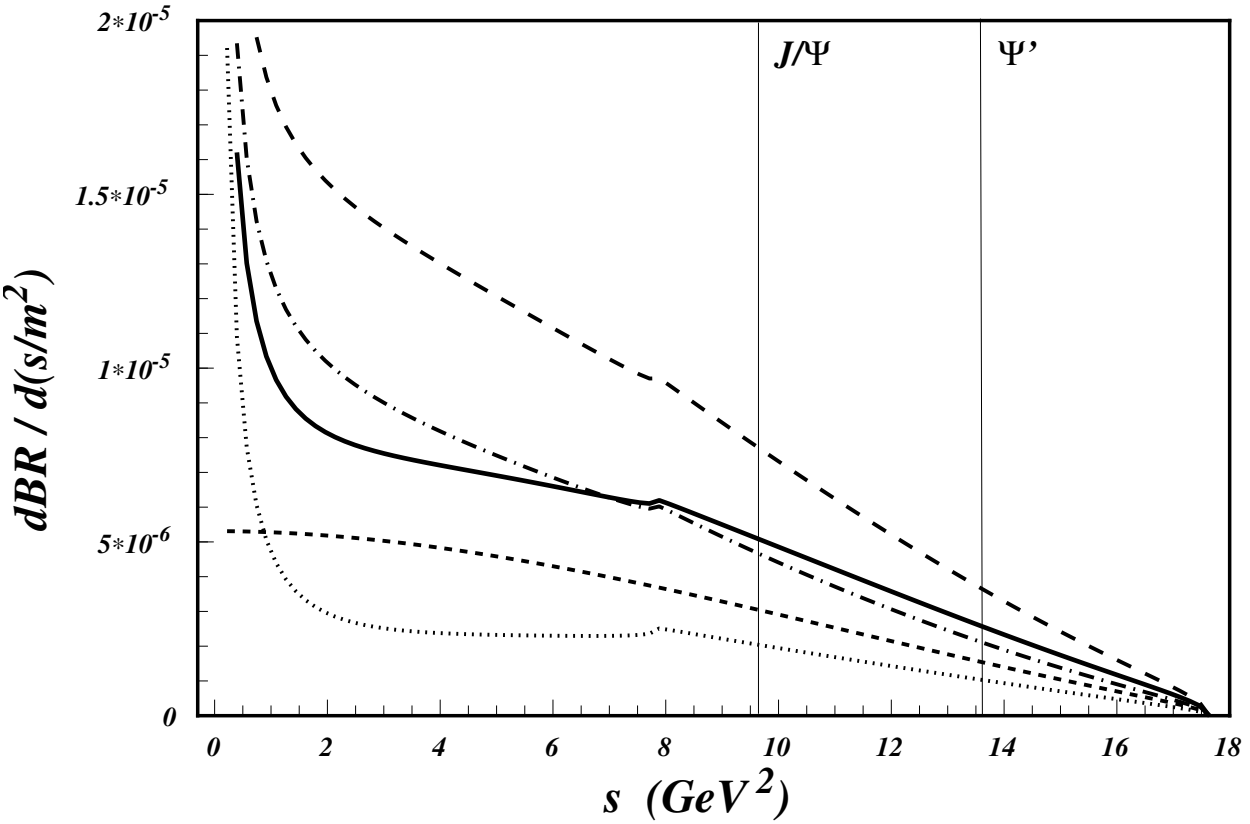

Figure 6: The dependence of the invariant-mass spectrum on the Wilson coefficients. Solid line: SM. Long-dashed line: $C_7 \to -C_7$, with other coefficients retaining their SM values. Short-dashed line: The contribution of C_{10} only. Dotted line: $C_{10} = 0$, with other coefficients retaining their SM values. Dash-dotted line: same as for the dotted one, but with $C_7 = -0.3$. The vertical lines indicate the location of the J/Ψ and Ψ' resonances.

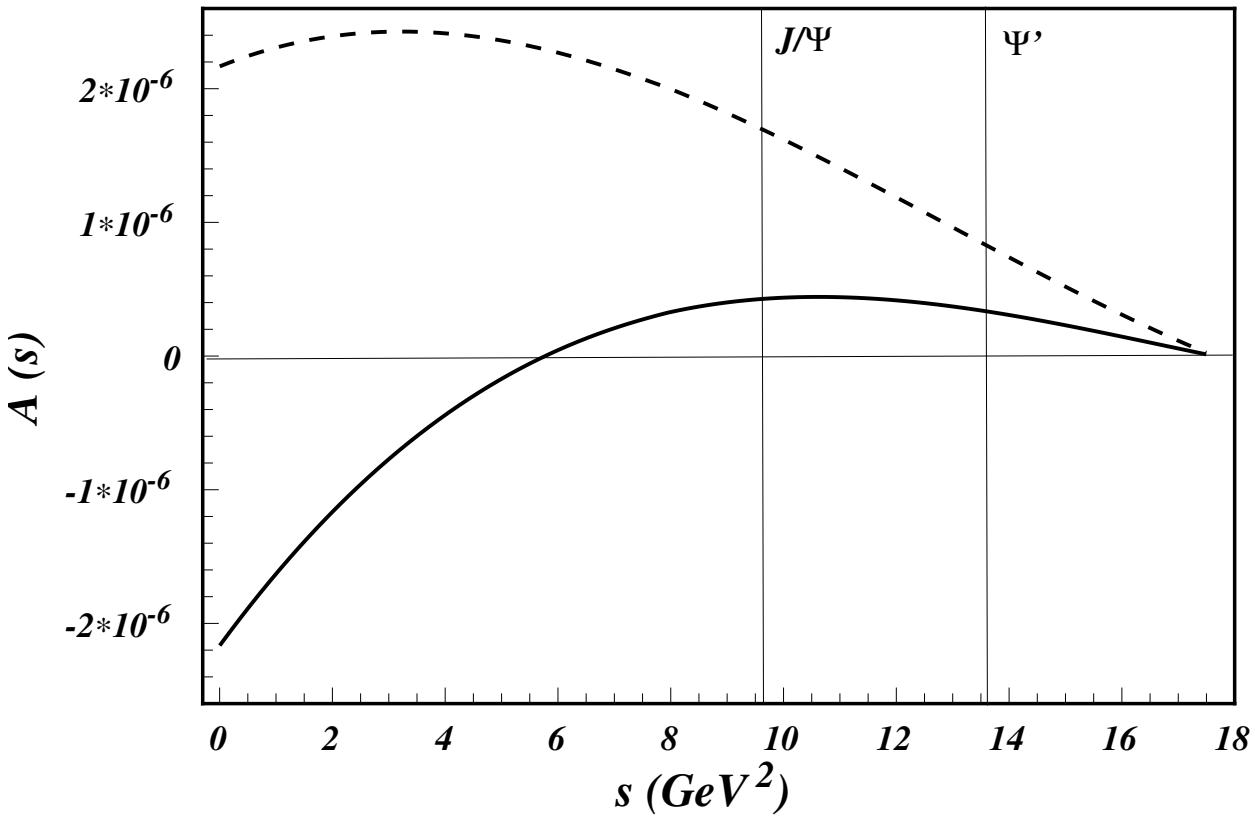

Figure 7: The dependence of the differential FB asymmetry on the Wilson coefficients. Solid line: SM. Long-dashed line: $C_7 \to -C_7$, with the other parameters retaining their SM values. The vertical lines indicate the location of the J/Ψ and Ψ' resonances.

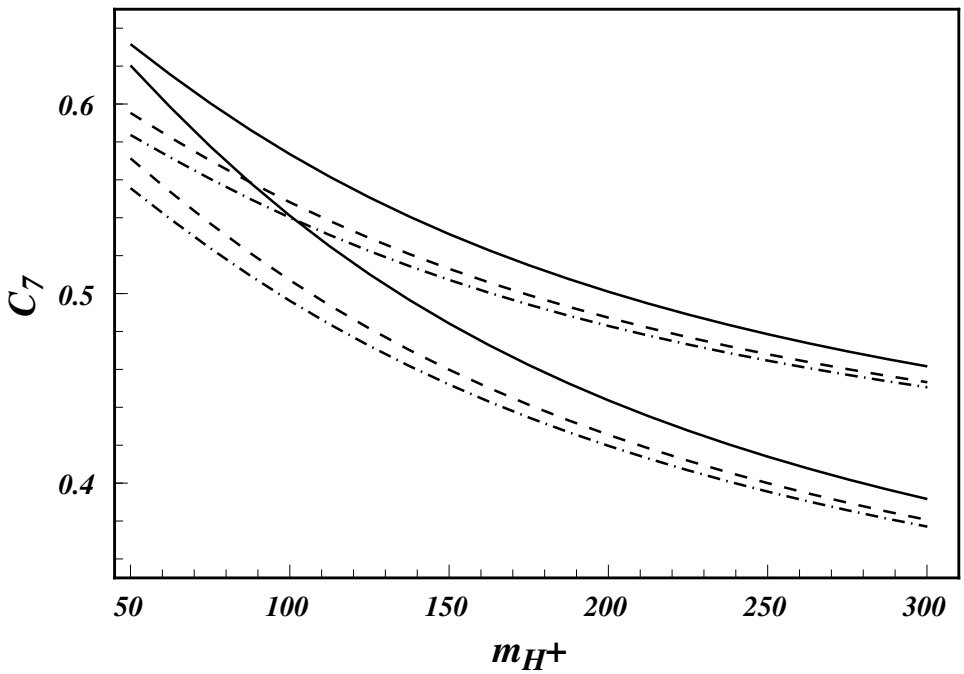

Figure 8: The dependence of C_7 on the charged Higgs mass for $v_2/v_1 = 1$ (solid line), $v_2/v_1 = 2$ (dashed line), $v_2/v_1 = 10$ (dot-dashed line). The band between the two curves reflects the QCD uncertainty (see text).

ceptable flavour violation in the K^0–$\bar{K}^0$ system. However, in the minimal supersymmetric model, flavour universality of the supersymmetry-breaking terms is usually assumed to hold at the grand-unification scale. In this case, a non-vanishing (and calculable) generation mixing in the quark-squark-gluino vertex is induced only by the effect of renormalization from the grand-unification scale to the weak scale. Given the present experimental limit on the gluino mass, this effect leads only to very small contributions to flavour-changing $b$decays [7] and it will be neglected in our analysis. Gluino-mediated flavour-changing neutral currents may however play an important role in non-minimal supersymmetric models (see [44] and references therein).

Once the gluino contributions (as well as the analogous ones from neutralino exchange) are neglected, the flavour violation in the model is completely specified by the familiar CKM matrix. The one-loop supersymmetric corrections to the Wilson coefficients C_7, C_9, and C_{10} are given by two classes of diagrams: charged-Higgs exchange and chargino exchange. Their analytical expressions can be found in ref. [7], and will not be repeated here.

The charged-Higgs contribution is specified by two input parameters: the charged-Higgs mass (m_{H^+}) and the ratio of Higgs vacuum expectation values ($v_2/v_1 \equiv \tan\beta$). This contribution is interesting in itself, since it corresponds to a well-defined SM extension: the 2DHM. The interaction between the

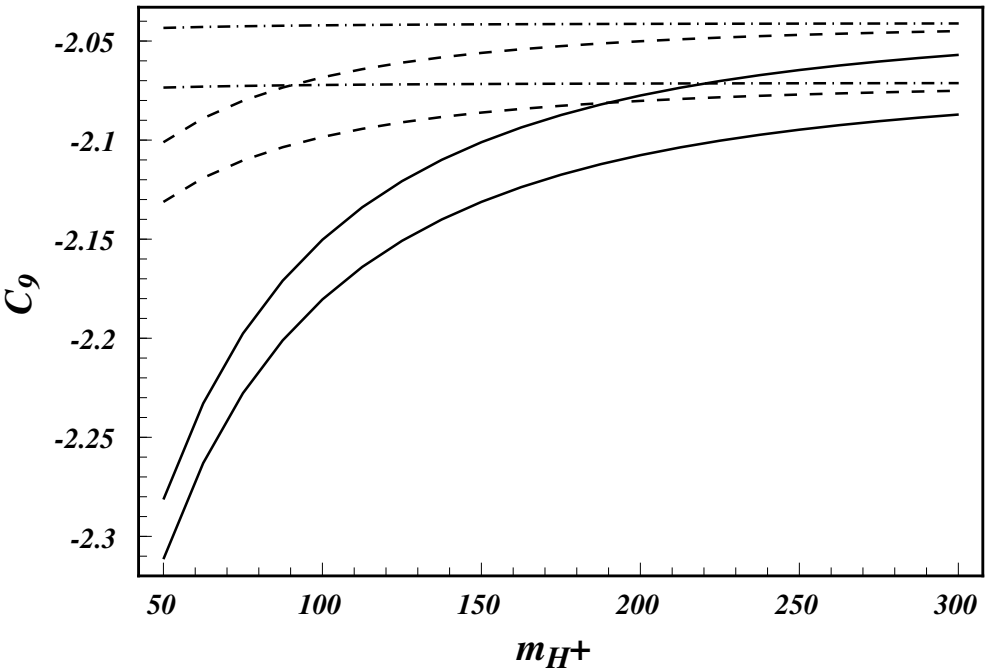

Figure 9: The dependence of C_9 on the charged Higgs mass. The notation is the same as in fig. 8.

charged Higgs and quarks is given by:

$$\mathcal{L} = \frac{g}{\sqrt{2}m_W} H^+ \bar{u} \left(A_u M_u V \frac{1-\gamma_5}{2} + A_d V M_d \frac{1+\gamma_5}{2} \right) d + \text{h.c.}, \tag{39}$$

where $M_{u,d}$ are the up and down quark mass matrices and V is the CKM matrix. If both up and down quarks get masses from the same Higgs doublet (this case is usually referred to as Model I), then

$$A_u = -A_d = 1/\tan\beta. \tag{40}$$

In the supersymmetric case, two different Higgs doublets couple separately to up and down quarks (Model II) and

$$A_u = 1/A_d = 1/\tan\beta. \tag{41}$$

Let us first consider the case relevant to supersymmetry, i.e. Model II. Figures 8, 9 and 10 show the charged-Higgs effects on C_7, C_9, and C_{10} for $m_t = 174$ GeV, at leading order in QCD. For each value of v_2/v_1, two curves for $\eta \equiv \alpha_s(M_Z)/\alpha_s(\mu)$ equal to 0.68 and 0.41 are shown. The band within the two lines reflects the QCD uncertainties, since the two chosen values of η correspond to the uncertainties in $\alpha_s(M_Z)$ $(= 0.118 \pm 0.006)$ [46] and μ $(m_b/2 < \mu < 2m_b)$. Recently the known part of the next-to-leading corrections has been included in the analysis of $b \to s\gamma$ [45]. They have the effect of reducing the scale dependence, and of decreasing considerably the value of C_7 with respect to the leading-order calculation shown in fig. 8. We expect

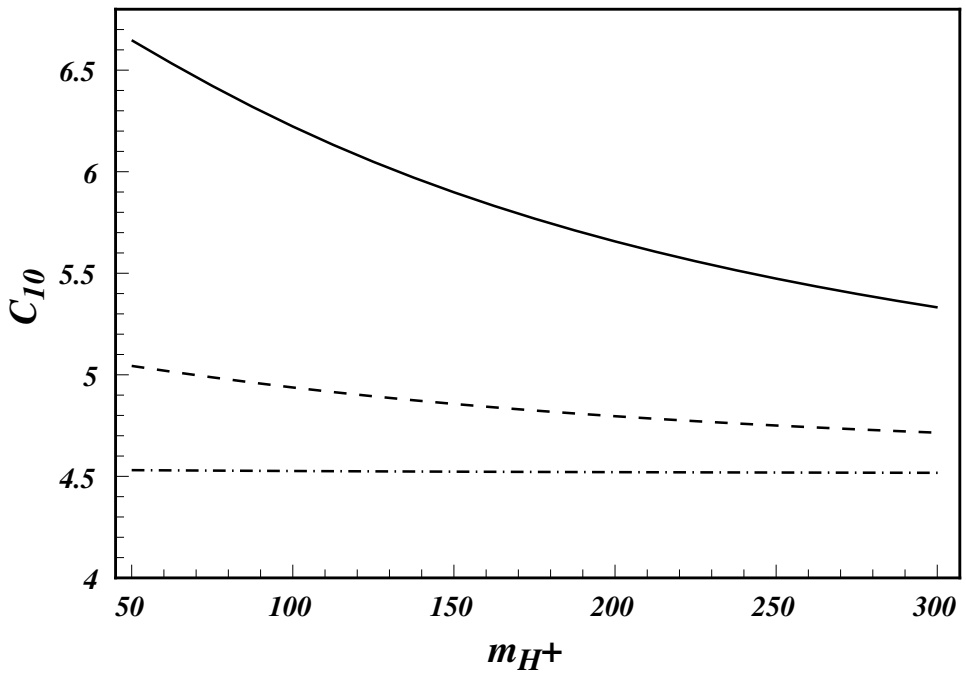

Figure 10: The dependence of C_{10} on the charged Higgs mass. The notation is the same as in fig. 8.

that we can safely ignore the next-to-leading corrections to C_9, because the QCD running is much less important here than in C_7. Note that C_{10} does not get renormalized under QCD.

The constraints imposed by supersymmetry on the scalar potential require $\tan\beta > 1$ and $m_{H^+} > m_W$. Notice that, as $\tan\beta$ becomes large, C_9 and C_{10} rapidly converge to the SM value (as $\tan^{-2}\beta$), while the charged-Higgs contribution to C_7 remains non-vanishing even in the limit $\tan\beta \to \infty$. In the case of a non-supersymmetric Model II, the experimental limit on $BR(b \to s\gamma)$ rules out a large region of the $\tan\beta$–m_H^+ parameter space [4, 6]. As a consequence, no significant deviation from the SM values of C_9 and C_{10} can be expected. In supersymmetry, however, the chargino can largely compensate for the charged-Higgs contribution to C_7 [8], and more decisive differences from the SM are foreseeable, as discussed below.

In the case of Model I, the expressions for C_9 and C_{10} are still the same as in Model II. However C_7 is modified and the constraint from $BR(b \to s\gamma)$ on the parameter space is much weaker. For $\tan\beta < 1$, C_7 can become negative. For small m_{H^+} and $\tan\beta$, it is possible to reach values for which C_7 equals, in absolute value, the SM prediction, but is opposite in sign. The region of parameter space where this happens is barely allowed by the constraints from ϵ_K and B^0–$\bar{B}^0$ mixing [47], but leads to unacceptable corrections to the $Z^0 \to \bar{b}b$ width [48] and is thus ruled out experimentally.

In addition to the diagrams with charged-Higgs exchange, the MSSM leads also to chargino-mediated diagrams. The chargino contribution is spec-

ified by six parameters. Three of them enter the 2×2 chargino mass matrix:

$$m_{\chi^+} = \begin{pmatrix} M & m_W \sqrt{2} \sin\beta \\ m_W \sqrt{2} \cos\beta & \mu \end{pmatrix}. \tag{42}$$

Following standard notations, we call $\tan\beta$ the ratio of vacuum expectation values, the same that appears also in the charged-Higgs sector, and M, μ the gaugino and higgsino mass parameters, subject to the constraint that the lightest chargino mass satisfies the LEP bound, $m_\chi^+ > 45$ GeV. The squark masses

$$m^2_{\tilde{q}^2_\pm} = \widetilde{m}^2 + m_q^2 \pm A \widetilde{m} m_q \tag{43}$$

contain two additional free parameters besides the known mass of the corresponding quark m_q: a common supersymmetry-breaking mass $\widetilde{m}$ and the coefficient A. The parameter A contains all the information (both from the μ-term and the trilinear term) of left-right squark mixing and it is constrained by the requirement that the lightest stop is not produced at LEP, $m_{\tilde{t}} > 45$ GeV [4]. We also take into account the CDF limit on squark masses [49], and impose $\widetilde{m} > 126$ GeV. In eq. (43) we have made the simplifying assumption that the supersymmetry-breaking left- and right-squark masses are equal. The last parameter included in our analysis is a common mass $m_{\tilde{l}}$ for sleptons, all taken to be degenerate in mass, with the constraint $m_{\tilde{l}} > 45$ GeV. Therefore the version of the MSSM we are considering is defined in terms of seven free parameters.

We have computed the Wilson coefficients in the MSSM and then varied the seven above-defined parameters in the experimentally allowed region. The results of our analysis are presented in fig. 11, which shows the regions of the C_9–C_{10} plane allowed by possible choices of the MSSM parameters. The upper plot of fig. 11 corresponds to parameters which give rise to positive (same sign as in the SM) values of C_7, consistent with experimental results on $b \to s\gamma$ ($0.19 < C_7 < 0.32$), while the lower plot corresponds to values of C_7 with opposite sign ($-0.32 < C_7 < -0.19$). We also show how our results are affected by an improvement in the experimental limits on supersymmetric particle masses, as can be expected from the Tevatron and LEP 200. Fig. 11 also shows the $C_9 - C_{10}$ regions allowed by the MSSM if the further constraints $m_{H^+} > 150$ GeV, $m_{\tilde{t}},\ m_{\chi^+},\ m_{\tilde{l}} > 100$ GeV are imposed.

The regions shown in fig. 11 illustrate the typical trend of the supersymmetric corrections. If supersymmetric particles exist at low energies, we can expect larger values of C_{10} and smaller (negative) values of C_9 than those predicted by the SM. This is the general feature, although the exact boundaries of the allowed regions depend on the particular model-dependent assumptions one prefers to use. For instance, the allowed regions can be slightly expanded if one introduces more general stop mixings than those

[4] For a particular choice of the mixing between the two stop states, the light stop can be decoupled from the Z^0 and the LEP bound would not apply. We disregard here this possibility.

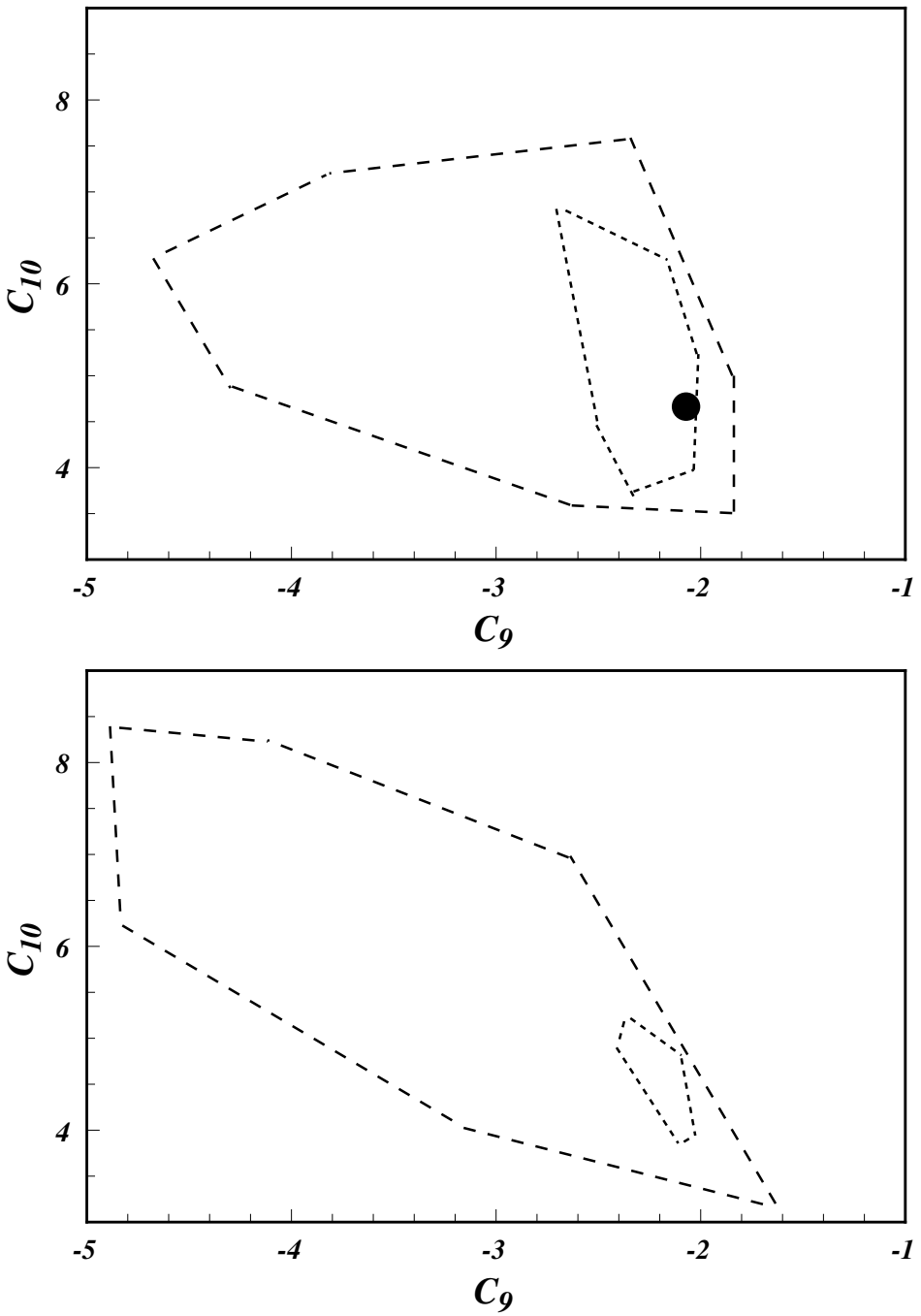

Figure 11: The region in the C_9-C_{10} plane obtained by varying the MSSM parameters. The upper (lower) plot corresponds to solutions that satisfy the $b \to s\gamma$ experimental constraint with positive (negative) C_7 given in eq.(3) and the present bounds ($m_{H^+} > 80$ GeV, $\tilde{m}_t, m_{\chi^+}, \tilde{m}_\ell > 45$ GeV). The smaller areas limited by the short-dashed line correspond to the region of the MSSM parameter space that will survive an unsuccessful search for supersymmetry at the Tevatron and LEP 200 ($m_{H^+} > 150$ GeV, $m_{\tilde{t}},\ m_{\chi^+},\ m_{\tilde{l}} > 100$ GeV).

considered here. On the other hand, if further constraints are imposed on the model (such as particular boundary conditions at the GUT scale, radiative symmetry-breaking, etc.), some of the parameters which in our analysis were taken as independent variables become related with each other, and the allowed region may somewhat shrink. However, the most interesting feature of supersymmetry is that solutions with negative values of C_7 are possible and are still consistent with present data. Moreover, values of the other two coefficients C_9 and C_{10} sufficiently different from the SM are allowed, leading to measurable differences in the decay rates and distributions of $B \to X_s \ell^+ \ell^-$ and $B_s \to \ell^+ \ell^-$.

5 Concluding Remarks

The branching ratios $\mathcal{B}(B \to K^* \gamma)$ and $B \to X_s \gamma$ have provided first measurements of the strength of the effective magnetic moment operator $m_b \bar{s}_L \sigma_{\mu\nu} b_R F^{\mu\nu}$. The inferred value of the Wilson coefficient $|C_7(m_b)|$ =0.19 – 0.32 from present data is in broad agreement with the SM estimate of the same. This, in turn, has led to rather stringent bounds on the parameters of a number of models. The comparison between the SM and experiment has become more precise with the measurement of the inclusive rate $\mathcal{B}(B \to X_s \gamma)$. There is an overriding need to firm up theoretical estimates in the SM by calculating the next-to-leading-order effects.

While the first step in the measurements of rare B decays has been made, we expect this field to undergo a qualitative change as the anticipated experimental facilities for B physics take shape and start producing B hadrons in large quantities. We have in mind here a steady consolidation of the CLEO and CDF data, with big strides expected to be made at the threshold B factories at SLAC and KEK and experimental facilities with proton beams such as HERA-B and in particular the LHC. Among others, we expect measurements of the CKM-suppressed radiative decays $B \to \rho \gamma$ and $B \to \omega \gamma$, and the FCNC semileptonic and leptonic decays $B \to X_s \ \ell^+ \ell^-$ (and the corresponding exclusive decays $B \to (K, K^*) \ell^+ \ell^-$) and $B_s^0 \to \ell^+ \ell^-$ at these facilities. Also, the nature of rare B-decay measurements will evolve in time from being exploratory to becoming rather precise. This has encouraged us to propose undertaking a more ambitious programme of extracting from data model-independent quantities – very much along the same lines as was carried out for the precision electroweak analysis of the LEP, SLC and low-energy data.

The electroweak precision tests, at LEP and elsewhere, have concentrated on the self-energies of the electroweak gauge bosons (γ, Z^0 and $W^\pm$), with possible deviations from the SM expressed in terms of a limited number of parameters [50, 51]. The main interest in rare B decays is to measure the

effective FCNC vertices to test the SM precisely and search for new physics. We have argued how to parametrize these vertices through a limited number of effective parameters, which govern the rates and shapes (differential distributions) in rare B decays $B \to X_s\gamma$, $B \to X_s\ \ell^+\ell^-$and $B_s \to \ell^+\ell^-$. The search for physics beyond the SM in these decays can be carried out in terms of three effective parameters, which can then be interpreted in a large class of models. The presence of non-SM physics may manifest itself by distorting the differential distributions in $B \to X_s\ \ell^+\ell^-$. Some possible examples of such distortions have been worked out. While the analysis presented here covers a large class of models, we have also presented profiles of the Wilson coefficients in the best-motivated extensions of the SM, namely the MSSM. We have pointed out that there exist two distinct solutions corresponding to the negative and positive values for $C_7(\mu)$, which cannot be distinguished from the data on $\mathcal{B}(B \to X_s\gamma)$, but they give rise to very different distributions in the decay $B \to X_s\ \ell^+\ell^-$. Moreover, the coefficients of the operators $C_9(\mu)$ and $C_{10}(\mu)$ for the MSSM models may attain values sufficiently different from the corresponding SM values. An encouraging result of our analysis is that rare B decays $B \to X_s\gamma$ and $B \to X_s\ \ell^+\ell^-$ have a discovery potential much beyond direct searches at these facilities. Finally, we remark that the purely leptonic decay modes $B_s^0 \to \ell^+\ell^-$ can also be used to further pin down the coefficient of the operator $\mathcal{O}_{10}$ involving the axial-vector leptonic current, i.e. $|C_{10}(\mu)|$, although this may require much larger B-hadron statistics. Precision measurements in rare B decays must be pursued vigorously.

Acknowledgements

We would like to thank Volodya Braun, Christoph Greub, Matthias Jamin, Guido Martinelli and Mikolaj Misiak for helpful discussions and correspondence.

References

[1] R. Ammar et al. (CLEO Collaboration), Phys. Rev. Lett. **71** (1993) 674.

[2] E. Thorndike (CLEO Collaboration), in Proc. of the American Physical Society Meeting, Washington (DC), April 1993; T. Browder, K. Honscheid and S. Playfer, Cornell report CLNS 93/1261,UH-511-778-93, OHSTPY-HEP-E-93-018, HEPSY 93-10 (1993).

[3] A. Ali and C. Greub, Z. Phys. **C60** (1993) 433.

[4] J.L. Hewett, Phys. Rev. Lett. **70** (1993) 1045; V. Barger, M.S. Berger, and R.J.N. Phillips, Phys. Rev. Lett. **70** (1993) 1368.

[5] T. Hayashi, M. Matsuda and M. Tanimoto, Kogakkan Univ. Report AUE-01-93 (1993).

[6] A.J. Buras, M. Misiak, M. Münz, and S. Pokorski, Munich preprint MPI-Ph/93-77; TUM-T31-50/93 (1993).

[7] S. Bertolini, F. Borzumati, A. Masiero, and G. Ridolfi, Nucl. Phys. **B353** (1991) 591.

[8] R. Barbieri and G.F. Giudice, Phys. Lett. **B309** (1993) 86.

[9] N. Oshimo, Nucl. Phys. **B404** (1993) 20;
R. Garisto and J.N. Ng, Phys. Lett. **B315** (1993) 372;
M.A. Diaz, Phys. Lett. **B322** (1994) 207;
F. Borzumati, preprint DESY-93-090 (1993);
S. Bertolini and F. Vissani, preprint SISSA 40/94/EP (1994);
P. Nath and R. Arnowitt, preprint CERN-TH.7214/94 (1994);
F. Borzumati, M. Drees, and M.M. Nojiri, preprint KEK-TH-400 (1994);
J. Lopez, D.V. Nanopoulos, X. Wang, and A. Zichichi, preprint CERN-TH.7335/94 (1994).

[10] J.L. Hewett, preprint SLAC-PUB-6521 (1994).

[11] T.G. Rizzo, preprint SLAC-PUB-6427 (1994).

[12] B. Barish et al., (CLEO Collaboration), Contribution to the International Conference on High Energy Physics, Glasgow, July 20–27, 1994, preprint CLEO CONF 94-1.

[13] N. Cabibbo, Phys. Rev. Lett. **10** (1963) 531; M. Kobayashi and T. Maskawa, Prog. Theor. Phys. **49** (1973) 652.

[14] T. Altomari, Phys. Rev. **D37** (1988) 677;
N.G. Deshpande et al., Z. Phys. **C40** (1988) 369;
P.J. O'Donnell and H.K.K. Tung, Phys. Rev. **D44** (1991) 741;
A. Ali, T. Ohl and T. Mannel, Phys. Lett. **B298** (1993) 195;
T. Hayashi et al. in [5].

[15] P. Ball, Munich report TUM-T31-43/93.

[16] P. Colangelo et al., Univ. of Bari Report BARI-TH/93-150 (1993).

[17] A. Ali, V.M. Braun and H. Simma, preprint CERN-TH.7118/93 (to appear in Z. Phys. C).

[18] S. Narison, preprint CERN-TH.7166/94, PM94/06 (1994).

[19] C. Bernard, P. Hsieh and A. Soni, Nucl. Phys. (Proc. Suppl.) **26** (1992) 347 and Univ. Washington Report Wash. U. HEP/93-35 (1993).

[20] K.C. Bowler et al. (UKQCD Collaboration), Edinburgh preprint 93/258 (1993).

[21] M. Ciuchini et al., preprint CERN-TH.7283/94 (1994).

[22] F. Abe et al. (CDF Collaboration), preprint FERMILAB-PUB-94/097-E, Apr 1994.

[23] A. Ali, C. Greub and T. Mannel, DESY Report 93-016 (1993), and in *B-Physics Working Group Report, ECFA Workshop on a European B-Meson Factory*, eds.: R. Aleksan and A. Ali, ECFA report 93/151, DESY 93-053 (1993).

[24] A. Ali, T. Mannel and T. Morozumi, Phys. Lett. **B273** (1991) 505.

[25] B. Grinstein, M.J. Savage and M.B. Wise, Nucl. Phys. **B319** (1989) 271.

[26] W. Jaus and D. Wyler, Phys. Rev. **D41** (1990) 3405; D. Wyler (private communication).

[27] J. Chay, H. Georgi and B. Grinstein, Phy. Lett. **B247** (1990) 399.

[28] I.I. Bigi, N.G. Uraltsev and A.I. Vainshtein, Phys. Lett. **B293** (1992) 430; I.I. Bigi et al., Minnesota preprint TPI-MINN-92/67-T (1992).

[29] A. Falk, M. Luke and M.J. Savage, preprint SLAC-PUB-6317 (1993).

[30] A. Ali and C. Greub, Z. Phys. **C49** (1991) 431; Phys. Lett. **259B** (1991) 182.

[31] A. Ali and E. Pietarinen, Nucl. Phys. **B154** (1979) 519.

[32] G. Altarelli et al., Nucl. Phys. **B208** (1982) 365.

[33] C.S. Lim, T. Morozumi and A.I. Sanda, Phys. Lett. **B218** (1989) 343.

[34] C. Dominguez, N. Paver and Riazuddin, Phys. Lett. **B214** (1988) 459.

[35] N. Deshpande, Report OITS 413 (1989).

[36] T. Inami and C.S. Lim, Prog. Theor. Phys. **65** (1981) 297.

[37] M. Ciuchini et al., Phys. Lett. **B316** (1993) 127; preprint ROME 973/93 (1993).

[38] A. Buras, M.E. Lautenbacher, M. Misiak and M. Münz, Munich report MPI-Ph/94-11; TUM-T31-60/94 (1994) and references quoted therein.

[39] G. Beall, M. Bander and A. Soni, Phys. Rev. Lett. **48** (1982) 848;
G. Ecker, W. Grimus and H. Neufeld, Phys. Lett. **B127** (1983) 365;
R.N. Mohapatra, G. Senjanovic and M.D. Tran, Phys. Rev. **D28** (1983) 546;
F.J. Gilman and M.H. Reno, Phys. Rev. **D29** (1984) 937.

[40] G. Ecker and W. Grimus, Nucl. Phys. **B258** (1985) 328; Z. Phys. **C30** (1986) 293;
G. Altarelli and P. Franzini, Z. Phys. **C37** (1988) 271.

[41] P. Langacker and S.U. Sankar, Phys. Rev. **D40** (1989) 1569.

[42] D. London and D. Wyler, Phys. Lett. **B232** (1989) 503.

[43] M.J. Duncan, Nucl. Phys. **B221** (1983) 285;
J.F. Donoghue, H.P. Nilles, and D. Wyler, Phys. Lett. **B128** (1983) 55.

[44] J.S. Hagelin, S. Kelley, and T. Tanaka, Mod. Phys. Lett. **A8** (1993) 2737.

[45] G. Martinelli et al., preprint CERN-TH-7283-94 (1994).

[46] S. Bethke, invited talk at *QCD '94*, Montpellier, France, July 94.

[47] V. Barger, J.L. Hewett, and R.J.N. Phillips, Phys. Rev. **D41** (1990) 3421;
G. Buchalla et al., Nucl. Phys. **B355** (1991) 305.

[48] G. T. Park, Mod. Phys. Lett. **A 9** (1994) 321.

[49] F. Abe et al. (CDF Collaboration), Phys. Rev. Lett. **69** (1992) 3439.

[50] M. Peskin and T. Takeuchi, Phys. Rev. **D46** (1992) 381.

[51] G. Altarelli and R. Barbieri, Nucl. Phys. **B405** (1993) 3.

Appendix: The effective Hamiltonian for $B \to X_s\gamma$ and $B \to X_s\ell^+\ell^-$

The effective Hamiltonian is

$$H_{eff} = -\frac{4G_F}{\sqrt{2}} V_{ts}^* V_{tb} \sum_{i=1}^{10} C_i(\mu)\mathcal{O}_i(\mu), \tag{44}$$

where the operator basis is chosen to be

$$\mathcal{O}_1 = (\bar{s}_{L\alpha}\gamma_\mu b_{L\alpha})(\bar{c}_{L\beta}\gamma_\mu c_{L\beta}) \tag{45}$$

$$\mathcal{O}_2 = (\bar{s}_{L\alpha}\gamma_\mu b_{L\beta})(\bar{c}_{L\beta}\gamma_\mu c_{L\alpha}) \tag{46}$$

$$\mathcal{O}_3 = (\bar{s}_{L\alpha}\gamma_\mu b_{L\alpha}) \sum_{q=u,d,s,c,b} (\bar{q}_{L\beta}\gamma_\mu q_{L\beta}) \quad (47)$$

$$\mathcal{O}_4 = (\bar{s}_{L\alpha}\gamma_\mu b_{L\beta}) \sum_{q=u,d,s,c,b} (\bar{q}_{L\beta}\gamma_\mu q_{L\alpha}) \quad (48)$$

$$\mathcal{O}_5 = (\bar{s}_{L\alpha}\gamma_\mu b_{L\alpha}) \sum_{q=u,d,s,c,b} (\bar{q}_{R\beta}\gamma_\mu q_{R\beta}) \quad (49)$$

$$\mathcal{O}_6 = (\bar{s}_{L\alpha}\gamma_\mu b_{L\beta}) \sum_{q=u,d,s,c,b} (\bar{q}_{R\beta}\gamma_\mu q_{R\alpha}) \quad (50)$$

$$\mathcal{O}_7 = \frac{e}{16\pi^2} m_b (\bar{s}_{L\alpha}\sigma_{\mu\nu} b_{R\alpha}) F^{\mu\nu} \quad (51)$$

$$\mathcal{O}'_7 = \frac{e}{16\pi^2} m_s (\bar{s}_{R\alpha}\sigma_{\mu\nu} b_{L\alpha}) F^{\mu\nu} \quad (52)$$

$$\mathcal{O}_8 = \frac{g}{16\pi^2} m_b (\bar{s}_{L\alpha} T^a_{\alpha\beta}\sigma_{\mu\nu} b_{R\alpha}) G^{a\mu\nu} \quad (53)$$

$$\mathcal{O}'_8 = \frac{g}{16\pi^2} m_s (\bar{s}_{R\alpha} T^a_{\alpha\beta}\sigma_{\mu\nu} b_{L\alpha}) G^{a\mu\nu} \quad (54)$$

$$\mathcal{O}_9 = (\bar{s}_{L\alpha}\gamma_\mu b_{L\alpha})(\bar{\ell}\gamma_\mu \ell) \quad (55)$$

$$\mathcal{O}_{10} = (\bar{s}_{L\alpha}\gamma_\mu b_{L\alpha})(\bar{\ell}\gamma_\mu\gamma_5 \ell) \quad (56)$$

$$(57)$$

where

$$q_L = \frac{1-\gamma_5}{2} q \text{ and } q_R = \frac{1+\gamma_5}{2} q. \quad (58)$$

The Wilson coefficients of the operators are given by the renormalization group evolution

$$\left[\mu\frac{\partial}{\partial\mu} + \beta(g)\frac{\partial}{\partial g}\right] C_i\left(\frac{M_W^2}{\mu^2}, g\right) = \hat{\gamma}_{ji}(g) C_j\left(\frac{M_W^2}{\mu^2}, g\right). \quad (59)$$

To leading logarithmic level, the QCD beta function $\beta(g)$ is given by

$$\beta(g) = -\beta_0 \frac{g^3}{16\pi^2} \quad \text{with} \quad \beta_0 = 11 - \frac{2}{3} f \quad (60)$$

and $\hat{\gamma}(g)$ is the anomalous dimension matrix, which is, to leading logarithmic acuracy, given by

$$\hat{\gamma}(g) = -\gamma_0 \frac{g^2}{16\pi^2} \quad (61)$$

Here γ_0 is a 10×10 matrix given by

$\gamma_0 =$

$$\left[\begin{array}{cccccccccc}
-2 & 6 & 0 & 0 & 0 & 0 & 0 & 3 & -\frac{16}{3} & 0 \\
6 & -2 & -\frac{2}{9} & \frac{2}{3} & -\frac{2}{9} & \frac{2}{3} & \frac{416}{81} & \frac{70}{27} & -\frac{16}{9} & 0 \\
0 & 0 & -\frac{22}{9} & \frac{22}{3} & -\frac{4}{9} & \frac{4}{3} & -\frac{464}{81} & \frac{140}{27}+3f & -\frac{16}{3}\left(u-\frac{d}{2}-\frac{1}{3}\right) & 0 \\
0 & 0 & 6-\frac{2}{9}f & -2+\frac{2}{3}f & -\frac{2}{9}f & \frac{2}{3}f & \frac{416}{81}u-\frac{232}{81}d & 6+\frac{70}{27}f & -\frac{16}{3}\left(u-\frac{d}{2}-3\right) & 0 \\
0 & 0 & 0 & 0 & 2 & -6 & \frac{32}{9} & -\frac{14}{3}-3f & -\frac{16}{3}\left(u-\frac{d}{2}\right) & 0 \\
0 & 0 & -\frac{2}{9}f & \frac{2}{3}f & -\frac{2}{9}f & -16+\frac{2}{3}f & -\frac{448}{81}u+\frac{200}{81}d & -4-\frac{119}{27}f & -\frac{16}{9}\left(u-\frac{d}{2}\right) & 0 \\
0 & 0 & 0 & 0 & 0 & 0 & \frac{32}{3} & 0 & 0 & 0 \\
0 & 0 & 0 & 0 & 0 & 0 & -\frac{32}{9} & \frac{28}{3} & 0 & 0 \\
0 & 0 & 0 & 0 & 0 & 0 & 0 & 0 & 0 & 0 \\
0 & 0 & 0 & 0 & 0 & 0 & 0 & 0 & 0 & 0
\end{array}\right]$$

Using as initial condition $C_j(M_W) = 0$ for $j = 1, 3, \cdots 6$ we obtain, for the solution of the renormalization group flow

$$C_1(\mu) = \frac{1}{2}C_2(M_W)\left(\eta^{6/23} - \eta^{-12/23}\right) \tag{62}$$

$$C_2(\mu) = \frac{1}{2}C_2(M_W)\left(\eta^{6/23} + \eta^{-12/23}\right) \tag{63}$$

$$\begin{aligned} C_3(\mu) = {} & C_2(M_W)\Big(-0.0112\eta^{0.8994} + \frac{1}{6}\eta^{-12/23} - 0.1403\eta^{-0.4230} + 0.0054\eta^{0.1456} \\ & - 0.0714\eta^{6/23} + 0.0509\eta^{0.4086}\Big) \end{aligned} \tag{64}$$

$$\begin{aligned} C_4(\mu) = {} & C_2(M_W)\Big(0.0156\eta^{0.8994} - \frac{1}{6}\eta^{-12/23} + 0.1214\eta^{-0.4230} + 0.0026\eta^{0.1456} \\ & - 0.0714\eta^{6/23} + 0.0984\eta^{0.4086}\Big) \end{aligned} \tag{65}$$

$$C_5(\mu) = C_2(M_W)\left(-0.0025\eta^{-0.8994} + 0.0117\eta^{-0.4230} + 0.0304\eta^{0.1456} - 0.0397\eta^{0.4086}\right) \tag{66}$$

$$C_6(\mu) = C_2(M_W)\left(-0.0462\eta^{-0.8994} + 0.0239\eta^{-0.4230} - 0.0112\eta^{0.1456} + 0.0335\eta^{0.4086}\right) \tag{67}$$

$$\begin{aligned} C_7(\mu) = {} & C_7(M_W)\eta^{16/23} + C_8(M_W)\frac{8}{3}\left(\eta^{14/23} - \eta^{16/23}\right) \\ & + C_2(M_W)\Big(-0.0185\eta^{-0.8994} - 0.0714\eta^{-12/23} - 0.0380\eta^{-0.4230} - 0.0057\eta^{0.1456} \\ & - 0.4286\eta^{6/23} - 0.6494\eta^{0.4086} + 2.2996\eta^{14/23} - 1.0880\eta^{16/23}\Big) \end{aligned} \tag{68}$$

$$\begin{aligned} C_8(\mu) = {} & C_8(M_W)\eta^{14/23} \\ & + C_2(M_W)\Big(-0.0571\eta^{-0.8994} + 0.0873\eta^{-0.4230} + 0.0209\eta^{0.1456} \\ & - 0.9135\eta^{0.4086} + 0.8623\eta^{14/23}\Big) \end{aligned} \tag{69}$$

$$\begin{aligned} C_9(\mu) = {} & C_9(M_W) + C_2(M_W)\Big(\frac{37}{33} - 0.0193\eta^{-0.8994} + \frac{74}{999}\eta^{-12/23} - 0.2608\eta^{-0.4230} \\ & - 0.0183\eta^{0.1456} - \frac{10}{9}\eta^{6/23} + 0.2143\eta^{0.4086}\Big) \end{aligned} \tag{70}$$

$$C_{10}(\mu) = C_{10}(M_W), \tag{71}$$

where

$$\eta = \frac{\alpha_s(M_W)}{\alpha_s(m_b)}$$

and we use $C_2(M_W) = -1$.

In terms of this effective Hamiltonian, the amplitude for $b \to s\ell^+\ell^-$ becomes

$$\begin{aligned} M &= 4\sqrt{2}G_F\frac{\alpha}{4\pi}(V_{ts}^*V_{tb})\left\{C_{9\,eff}\overline{s}_L\gamma_\mu b_L\overline{l}\gamma^\mu l + C_{10}\overline{s}_L\gamma_\mu b_L\overline{l}\gamma^\mu\gamma_5 l\right. \\ &\quad \left. -C_7\overline{s}i\sigma_{\mu\nu}\frac{q^\nu}{q^2}(m_s b_L + m_b b_R)\overline{l}\gamma^\mu l\right\}, \end{aligned} \tag{72}$$

where $q^\mu = p_1^\mu + p_2^\mu$ is the momentum transferred to the leptons. The effective coefficient $C_{9\,eff}$ contains the contributions from the one-loop matrix elements of $\mathcal{O}_1, ..., \mathcal{O}_6$ and is given by (8). This definition involves the one-loop function g, which is given by

$$\begin{aligned} \text{Re } g(z,s) &= -\frac{4}{9}\ln z^2 + \frac{8}{27} + \frac{16z^2}{9s} \\ &\quad -\frac{2}{9}\sqrt{1-\frac{4z^2}{s}}\left(2+\frac{4z^2}{s}\right)\ln\left|\frac{1+\sqrt{1-\frac{4z^2}{s}}}{1-\sqrt{1-\frac{4z^2}{s}}}\right| \quad \text{for } s > 4z^2 \end{aligned} \tag{73}$$

$$\begin{aligned} \text{Re } g(z,s) &= -\frac{4}{9}\ln z^2 + \frac{8}{27} + \frac{16z^2}{9s} \\ &\quad -\frac{2}{9}\sqrt{1-\frac{4z^2}{s}}\left(2+\frac{4z^2}{s}\right)\ \text{atan}\ \left(\frac{1}{\sqrt{\frac{4z^2}{s}-1}}\right) \quad \text{for } s < 4z^2 \end{aligned} \tag{74}$$

$$\text{Im } g(z,s) = -\frac{2\pi}{9}\sqrt{1-\frac{4z^2}{s}}\left(2+\frac{4z^2}{s}\right)\Theta(s-4z^2). \tag{75}$$